Orhan Yapici*, Marios Theofanous, Huanxin Yuan, Samir Dirar, Sheida Afshan. (2022) Numerical simulation and design of ferritic stainless steel bolted T-stubs in tension. Journal of Constructional Steel Research. https://doi.org/10.1016/j.jcsr.2022.107555

Numerical simulation and design of ferritic stainless steel bolted T-stubs in tension

Orhan Yapici[1*], Marios Theofanous[2], Huanxin Yuan[3], Samir Dirar[2], Sheida Afshan[4]

[1] *Institute for Infrastructure & Environment, Heriot-Watt University, Edinburgh, EH14 4AS, United Kingdom*

[2] *Department of Civil Engineering, University of Birmingham, Birmingham, B15 2TT, United Kingdom*

[3] *School of Civil Engineering, Wuhan University, Wuhan 430072, PR China*

[4] *Faculty of Engineering and Physical Sciences, University of Southampton, Southampton SO16 7QF, United Kingdom*

[*]corresponding author:

Orhan Yapici, *Institute for Infrastructure & Environment, Heriot-Watt University, Email: o.yapici@hw.ac.uk*

Abstract

Following the experimental study on EN 1.4003 ferritic stainless steel T-stubs in tension discussed in the companion paper, this study reports the development and validation of an advanced FE model that can predict the overall behaviour and failure modes of ferritic stainless steel bolted T-stubs subjected to tension. Key simulation strategies regarding the modelling of bolt geometry and overcoming numerical instabilities are discussed. Following the determination of material properties in the longitudinal, transverse and diagonal direction reported in the companion paper, the effect of allowing for anisotropy in the FE simulations is investigated and modelling recommendations for its inclusion in FE models are made. Moreover, the effect of bolt end and edge spacing on the joint plastic resistance, ultimate capacity, ductility as well as overall response is comprehensively discussed by inspecting the stress distribution through the plate thickness at various locations along the T-stub, thus revealing both the flexural and the membrane component of the load transfer mechanism. The numerical results were validated against the experimental results reported in the companion paper in terms of predicted plastic and ultimate resistance, ductility and obtained failure modes. On the basis of the obtained results and the discussion, modelling recommendations for the simulation of stainless steel T-stubs are made.

Keywords

Stainless steel, Ferritic, T-stub, Bolted connections, Numerical analysis, Material anisotropy.

1. Introduction

T-stubs in tension are key components in the modelling of the behaviour and design of tension zones of beam-to-column connections according to the component method framework of EN 1993-1-8 [1] and have therefore received widespread attention from researchers. In addition to experimental studies in the literature, there are several studies reported on the FE modelling of T-stubs connections. Bursi et al. [2], Zajdel [3] and Wanzeck et al. [4] investigated the behaviour of T-stub connections using FE model. An effective 2-D numerical model proposed by Mistakids et al. [5]. Moreover, advanced finite element models have been developed for the numerical analysis of T-stub connections by Swanson et al. [6] and Gantes et al. [7]. Coelho et al. [8,9] studied the non-linear behaviour of the T-stubs using a three-dimensional FE model with comprehensive parametric analyses. Furthermore, Herrera et al. [10] studied the performance of built-up T-stub for double T moment connections. Likewise, a series of numerical studies with developed FE models on the performance of the thick flange T-stubs has been reported by Hantouche et al. [11, 12]. In 2014, the effect of the flexural rigidity of the bolts on the response of T-stub connections has been studied using FE models by Abidelah et al. [13]. Additionally, a simplified FE model has been proposed in order to investigate the structural behaviour of T-stub connections by Francavilla et al. [14]. Similarly, Ceniceros et al. [15,16] developed a numerical information approach for investigating the ductile behaviour of the T-stub connections. In 2018, Kong et al. [17] developed a FE element model to predict the initial stiffness and ultimate moment of T-stub connections. Gödrich et al. [18] proposed the component based FE model in order to investigate the structural response of the T-stubs in tension.

The most of the published studies provide an extensive knowledge for the behaviour of carbon steel bolted connections and T-stubs in tension however, studies on stainless steel connections are very limited. Bouchaïr et al. [19], have investigated the ductility and ultimate behaviour of stainless steel bolted T-stubs with numerical investigations. The resistance predictions for stainless steel T-stubs according to EN 1993-1-8 [1] were very conservative and it was also stressed that extensive numerical and experimental researches should be conducted to confirm these conclusions. The first ever experimental studies on stainless steel T-stubs in tension were reported by Yuan et al. [20], who conducted 27 experimental tests on austenitic and duplex stainless steel T-stubs. It was concluded that the existing design rules defined in EN 1993-1-8 [1] provides overly conservative strength predictions for stainless steel bolted T-stubs [20]. Elflah et al. [21,22], have examined the behaviour of stainless steel moment resisting connections as well as stainless steel blind-bolted connections [23] with experimental and numerical studies. It was reported that the design provisions of EN 1993-1-8 [1], which specify design rules for carbon joints, that are also applicable for stainless steel joints [24], can predict the stiffness of the joints sufficiently accurate predictions but provides significantly conservative predictions for the strength [21-23]. Moreover, the structural behaviour of the moment resisting connections was investigated by three-dimensional FE model and the stiffness and resistance predictions were reported comprehensively, and proposed model validated using the experimental results [22]. Recently, Wang et al. [25], Bu et al. [26], Song et al. [27], Gao et al. [28,29], Yapici et al. [30-32] and Yuan et al. [33,34] conducted experimental and numerical studies on the behaviour of stainless steel connections and reported similar conclusions. The studies in the literature focused primarily on austenitic and duplex stainless steel grades, while the structural performance of ferritic stainless steel connections has not been studied to date. In order to fill this gap in the literature, the ultimate behaviour of ferritic stainless steel bolted T-stubs under tension has been studied by the authors and reported as a companion paper in reference [35]. According to recent experimental studies, the ferritic stainless steel T-stubs [35] display a different behaviour compared to their austenitic and duplex counterparts [33].

In the companion paper [35], 17 experimental tests on ferritic stainless steel T-stubs in tension were reported, thus augmenting the limited available data pool [20, 33] with the first ever ferritic stainless steel T-stub results ever to be reported. In this paper, recommendations for the numerical modelling of ferritic stainless steel T-stubs are provided. Following the observations on the pronounced anisotropy of ferritic stainless steel [35], the effect of material anisotropy is discussed in detail, whilst a comprehensive discussion on mesh size and analysis procedures is also included. Furthermore, the stress distribution developed on the flange to web junction at various load levels is inspected and the validity of current design assumptions regarding the development of stresses and the applicability of plastic design procedures is assessed. In line with the companion paper [35], the importance of membrane action at high deformations is highlighted and its importance on predicting the ultimate failure load is demonstrated.

2. Development of FE model

2.1. Modelling assumptions

Three-dimensional nonlinear finite element analyses were carried out using ABAQUS [36]. Because of the symmetry of the modelled T-stub in terms of geometry, applied load, boundary conditions and observed response, with respect to two planes, only a quarter of the T-stubs was explicitly modelled, as shown in Fig. 1, using the measured geometry reported in [35]. Since the presence of the fillet welds affects the exact location of the yield lines of the flange in the vicinity of the web, the size of the fillet welds needs to be explicitly considered. To this end, two modelling techniques were followed; one involving the separate modelling of the flange, the web and the fillet weld the tying of the relevant degrees of freedom at their interfaces and one where the whole T-stub including the weld was modelled as a solid cross-section and extruded along its length. Both techniques gave identical results. The 30 mm thick steel plate to which the specimens were bolted was also explicitly modelled as shown in Fig. 1.

To reduce computational cost, the threaded geometry of the bolt shank was simplified in the simulations as a cylindrical surface with an effective diameter such that the area of the simulated bolts equals the stress area of the threaded bolts, whilst the bolt heads and nuts were modelled as cylindrical instead of hexagonal discs. This modelling simplification of the bolt geometry has been shown to yield good results without compromising accuracy [6, 22, 37]. Furthermore, the bolt head, bolt nut and washers were simplified as cylinders and were tied to the bolt shank as is customarily done when simulating bolts [6, 22, 37-39]. No bolt preload was applied, given that in the tests the bolts were hand-tightened to obtain the snug-tight condition.

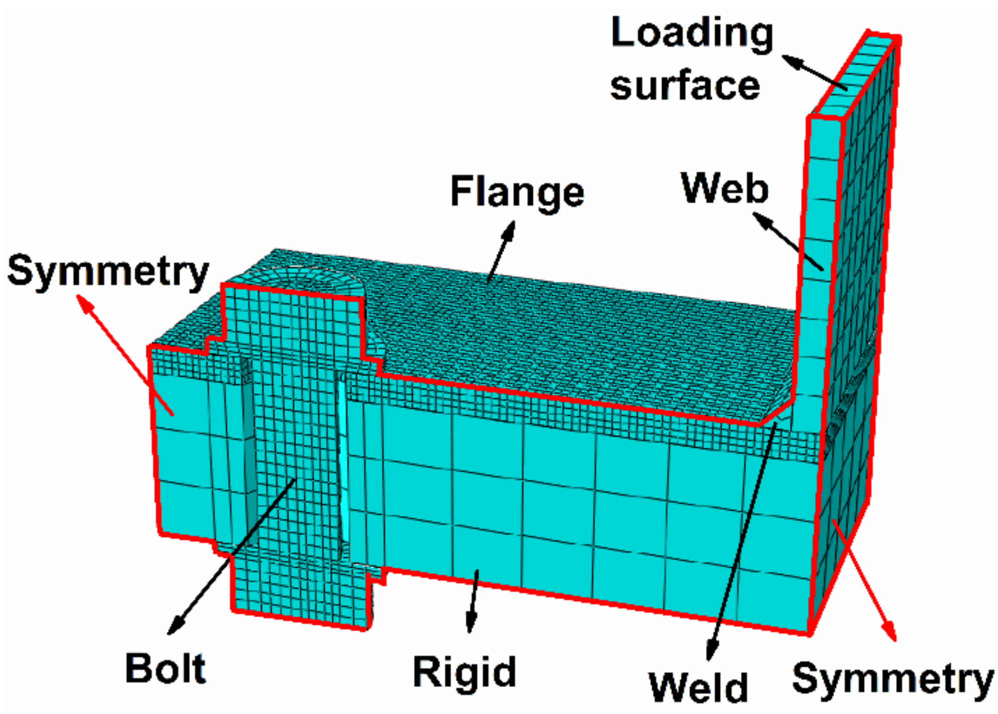

Fig. 1. The developed FE model for the analyses.

All parts were discretized with the eight-node linear brick element with reduced integration, C3D8R, as it was shown to provide good accuracy at a low computational cost compared to other elements [6, 22, 37-40]. Several mesh densities were tried, and a structured mesh was employed with varying mesh density in the different parts of the model. At least three elements were provided through the thickness of the T-stub to accurately capture their out-of-plane flexure and avoid the effect of shear locking. A minimum of 2 elements through the thickness of a flange in bending has been recommended in [39]. A more refined mesh was adopted around the smaller area of the bolt in order to more accurately simulate the interface bolt-T-stub interface and capture contact. The adequacy of the selected mesh size is discussed later on in the validation of the model.

Surface to surface contact, with finite sliding was assumed for all contact surfaces, namely bolt shank to bolt hole, bolt head to flange, bolt head to rigid plate are modelled thus enabling large slip to be simulated. The penalty friction method is adopted to simulate tangential behaviour, whilst hard contact is assumed for normal behaviour. The selected coefficient of friction was 0.3 and lies within the values of 0.2-0.33 recommended in the literature for steel, stainless steel and aluminium connections [22, 37-41]. Symmetry conditions with respect to two planes of symmetry were applied and only ¼ of the model was simulated as previously discussed. The model was loaded via a prescribed displacement at the top of the web of the T-stub, whilst all degrees of freedom of the bottom side of the thick elastic plate was restrained to provide reaction to the applied loading.

Due to the highly nonlinear behaviour of the model, brought about by the contact among its various parts, convergence difficulties emerged when a nonlinear static procedure was employed. To speed up the analysis and overcome the convergence difficulties, a quasi-static explicit dynamic analysis was employed as the selected analysis type. Mass scaling was utilized to reduce computational time, whilst quasi-static response was achieved by specifying a slow and smooth displacement rate and checking that the kinetic energy was smaller than 2% of the internal energy for the greatest part of the analysis, thus ensuring that inertia effects were insignificant. The selected analysis type did not compromise the accuracy of the simulations as discussed in section 3.

2.2. Material modelling and anisotropy

The nonlinear material properties of the stainless steel T-stubs and the bolts were modelled using the three stage Ramberg-Osgood model [42]. The material parameters for the ferritic stainless steel plates determined from tensile coupon tests as reported in the companion paper [35] were adopted herein. Likewise, the material properties of the stainless steel bolts reported in reference [35] were utilised.

The standard von Mises yield criterion with isotropic hardening is conventionally employed to simulate the plastic behaviour of metals when they can be considered isotropic. In order to incorporate the material anisotropy in the numerical analysis, material properties in the longitudinal, transverse and diagonal directions are required. In Table 1, the average nominal yield strength values as determined in Ref. [35], are reported for each direction. The anisotropy ratio, defined as the ratio of the 0.2% proof stress in a particular direction over the 0.2% proof stress in the rolling/longitudinal direction is also reported as a means to quantify the observed material anisotropy. The material exhibited a 0.2% proof stress in the transverse direction 21% and 7% higher than that in the longitudinal direction for 5 mm and 10 mm coupons, respectively. The anisotropy ratio values determined herein for the ferritic stainless steel plates is very similar to those found in the literature [43]. Hill's [44] yield potential is adopted as the yield criterion in the numerical models which account the material anisotropy. In order to establish the yield function considering the anisotropy, the six anisotropic yield stress ratios have to be defined. The six anisotropic yield stress ratios have been calculated using stress values reported for the 5 mm coupon tests as R11=1, R22=1.21, R33=R12=1.11, R13=R23=1 and for the 10 mm coupon tests as R11=1, R22=1.07, R33=R12=1.02, R13=R23=1. The effects of anisotropy on the obtained results are assessed in the next section. In Table 2, the material properties of two smooth cylindrical coupons which were machined from A4-80 stainless steel bolts are represented.

Table 1. Material properties of the ferritic stainless steel plates [35].

Coupon thickness	Direction	E_0 (MPa)	$\sigma_{0.2}$ (MPa)	$\sigma_{1.0}$ (MPa)	$\sigma_{2.0}$ (MPa)	σ_u (MPa)	ε_f (%)	$\varepsilon_{f,true}$	m	n	Anisotropy
10 mm	LT	189114	279.3	298.8	324.1	441.3	0.35	-	2.8	20	1.00
10 mm	TT	196983	298.4	321.3	348.1	462.9	0.10	-	2.8	25	1.07
10 mm	DT	192094	284.5	303.5	328.4	438.6	0.36	-	2.8	16	1.02
5 mm	LT	204266	337.1	367.3	378.6	426.3	0.32	1.35	2.8	6.3	1.00
5 mm	TT	192996	409.0	425.1	435.6	467.1	0.18	1.19	2.8	12	1.21
5 mm	DT	184125	375.3	390.1	399.4	436.6	0.25	1.22	2.8	13	1.11

Table 2. Material properties of the A4-80 stainless steel bolts [35].

#	E (MPa)	$\sigma_{0.2}$ (MPa)	$\sigma_{1.0}$ (MPa)	σ_u (MPa)	ε_u (%)	$n_{0-0.2}$	$n_{0.2-1.0}$	$n_{1.0-u}$
1	185000	410	600	727	0.19	4	4	11
2	179000	400	590	726	0.21	4	3	11

2.3. Modelling of fracture

As observed in the experimental tests, all T-stubs with a 5 mm thickness ultimately failed due to fracture of the ferritic T-stubs, in the vicinity of the bolt holes, whilst the bolts exhibited pronounced plastic deformation but no fracture due to the employed small thickness of the T-stub specimens compared to the bolt strength. Since no fracture characterisation studies were conducted for the ferritic stainless steel material, the fracture of the plates was not explicitly simulated in the analysis. In the absence of relevant material parameters, a simplified approach was followed, according to which fracture of the T-stub flange was not explicitly modelled but was indirectly defined based on longitudinal plastic strain at fracture ε_f given in Table 1. Hence, the T-stubs were assumed to fail when the equivalent plastic strain obtained from the analysis reached ε_f, at which point the analysis was discontinued. For models considering anisotropy, the average value of the strain at fracture obtained for the 3 directions (i.e. longitudinal, trnasverse and diagonal) was adopted as the strain limit of the material. An indirect definition of fracture based on strains values was successfully employed in similar studies investigating the fracture of stainless steel plates [45], as well as fracture of bolts in T-stubs [33, 8] and moment resisting connections [22, 28]. The FE analysis which is reported in section 3.1 does not contain any explicit fracture model for plates, instead previously explained approach was followed. However, in section 3.3 an explicit progressive damage model in ABAQUS were utilised for the stainless steel bolts. Parameters of ductile damage initiation criterion was derived from the fundamental behaviour of tensile test coupons which was reported in [35] in line with the proposed approach by Pavlovic et al. [46] (Fig. 2). Firstly, damage initiation criterion was defined as equivalent plastic strain at the onset of damage ($\varepsilon_{pl,D}$) in function of stress triaxiality (η) [46]. The expression given in Eq. (1) is for the relationship between equivalent plastic strain at damage initiation and the stress triaxiality which was derived using the experimental test results on A4-80 stainless steel bolts reported by Yapici et al. [35, 47] and it was utilised in the developed FE models reported in section 3.3. All the boundary conditions and contact definitions remain unchanged as in the previous sections FE models. It should be noted that the propagation of damage is ignored and instantaneous fracture of the bolts is assumed.

$$\varepsilon_{pl,D} = 0.46e^{-1.33\eta} \tag{1}$$

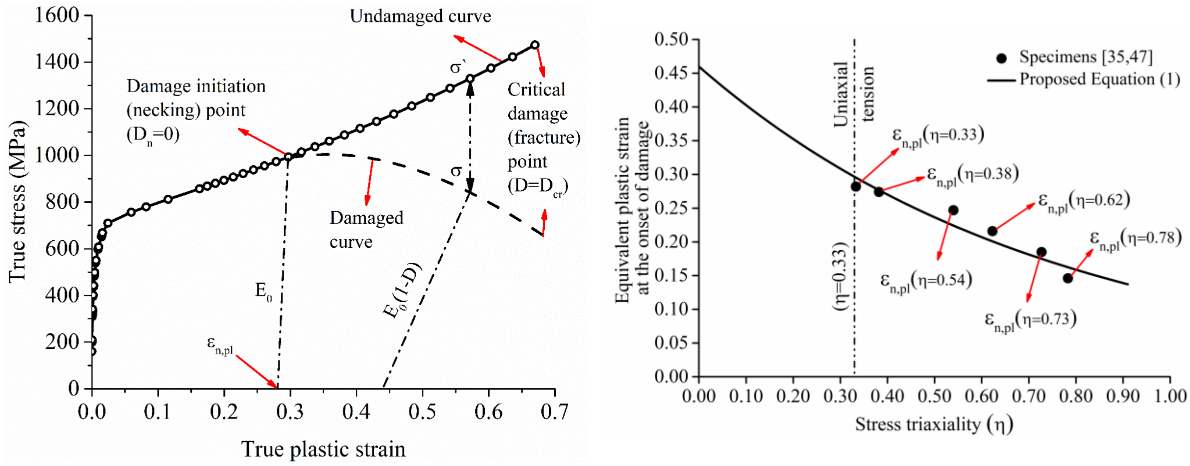

(a) Explanation of damage extraction (b) Damage initiation criterion

Fig. 2. Ductile damage parameters for stainless steel bolts.

3. Results and discussions

3.1. Validation of the FE models

The developed FE models were utilised to simulate the ferritic stainless steel bolted T-stubs tests [35] and the obtained numerical results were compared against the experimental ones. For each of the tested specimens, three analyses with different assumed material responses for the T-stubs were conducted to assess the effect of incorporating material anisotropy in the simulations. In two of the analyses isotropic material response was assumed; the longitudinal material properties were adopted for the first case and the transverse ones for the second; whilst in the third case the material anisotropy was explicitly incorporated via Hill's yield potential.

For all three analyses conducted, at least 3 solid elements through the flange thickness were adopted to capture the flexural deformations. The adequacy of the selected mesh density is verified by comparing the results obtained for a typical T-stub with 1 bolt row (S2) and a typical T-stub with 2 bolt rows (D1), as shown in Fig. 3. It can be concluded that the mesh element number through the thickness does not affect the response significantly and the curves obtained were almost identical. Similar results were obtained for the rest of the T-stub regardless of the assumed material properties.

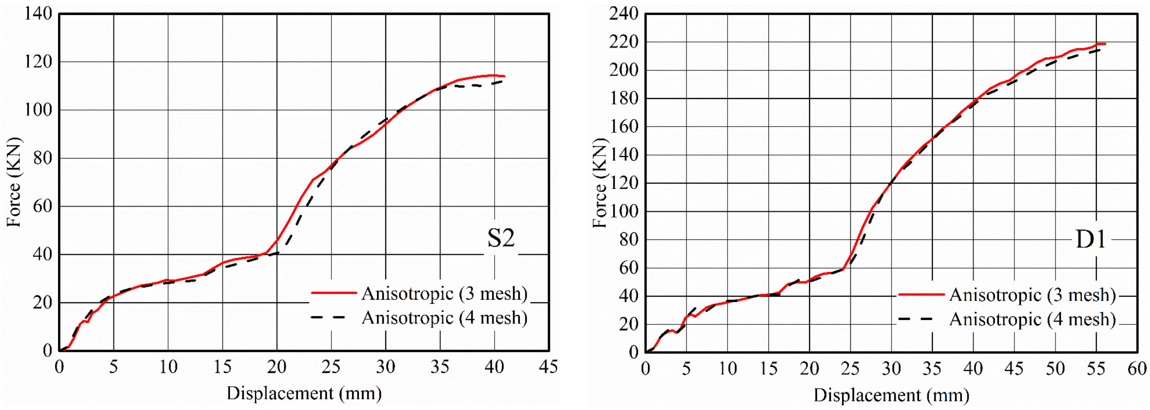

(a) (b)

Fig. 3. Numerical load-deformation curves with 3 and 4 elements through the flange thickness of a) S2 and b) D1.

To verify the appropriateness of using an (quasi-static) explicit dynamic analysis procedure to simulate the static response of the T-stubs, the analysis for specimens S2 and D1 were repeated using the general static solver and the obtained load-deformation responses are shown in Fig. 4, where a close agreement between the two curves can be observed throughout the loading history. It can thus be concluded the explicit dynamic analysis of a quasi-static problem and the general static analysis yield very similar results as long as the selected mass scaling and loading speed is such that no significant inertia effects occur [32]. In addition to checking that the kinetic energy is small compared to the potential energy, an easy means to assess whether the chosen mass scaling and loading speed is appropriate is to check that the resulting response is smooth without any notable fluctuations. The explicit dynamic analysis was chosen herein due to its superior computational speed and absence of convergence issues.

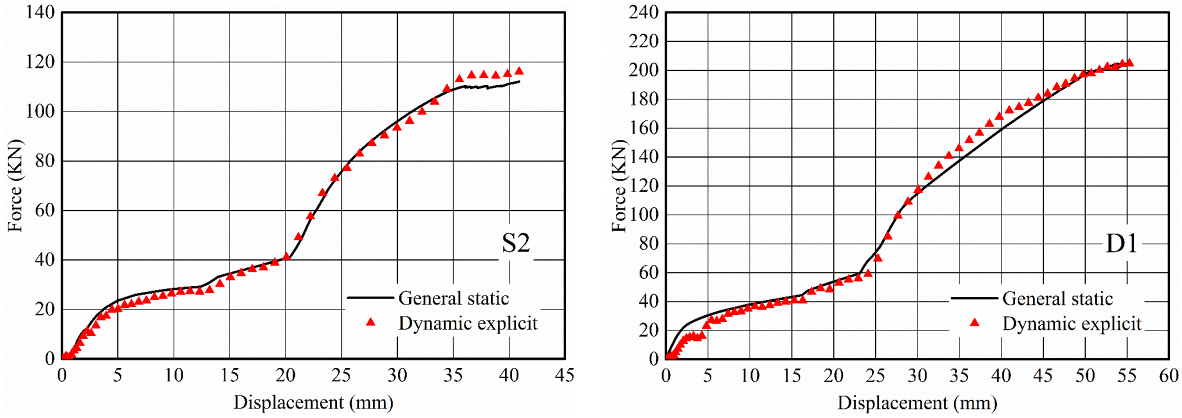

(a) (b)

Fig. 4. Numerical load-deformation response for static and explicit dynamic analysis of a) S2 and b) D1.

The comparisons between the FE predictions and the test results including the force-deformation curves and the failure modes of the specimens are presented in Fig. 5. It can be observed that the numerically predicted load-deformation curves are in close agreement with the experimental ones reported in the companion paper [35]. The anisotropic FE models significantly improve the accuracy of the predictions as evidenced by the load-displacement curves especially for the models of specimens S1, S2, D2, D3 and D6 with respect to the experimental response. For the rest of the specimens it seems the models employing isotropic material response with longitudinal material properties display the closest agreement with the test results. It should be noted that there is a discrepancy in the prediction of the initial stiffness of specimen S3 and ultimate force of S6, as the experimental stiffness appears significantly lower than the numerically predicted one for S3 and the experimental ultimate force is considerably higher than the numerically predicted ultimate force. These are attributed to a 3 mm gap between the ends of the T-stub and the rigid plate to which it was bolted due to welding induced thermal distortion of the specimen, which led to a delay in the development of the prying forces. This effect was not properly reflected in the FE models however Tartaglia et al. [48] examined the influence of constructional imperfections i.e. misalignment of the web and flange bowing namely non-perpendicularity between the web and flange due to the initial curve and concluded they have no significant effect on the predicted strength of the T-stubs..

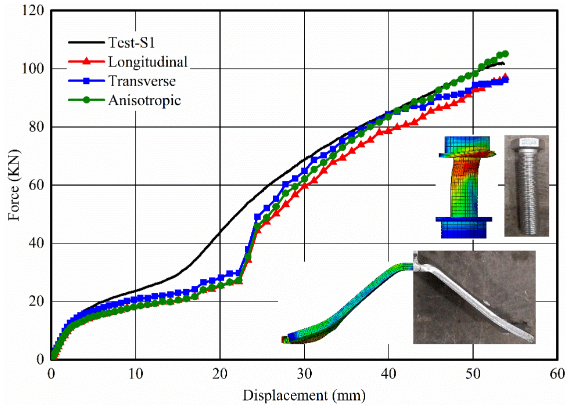

(a) S1

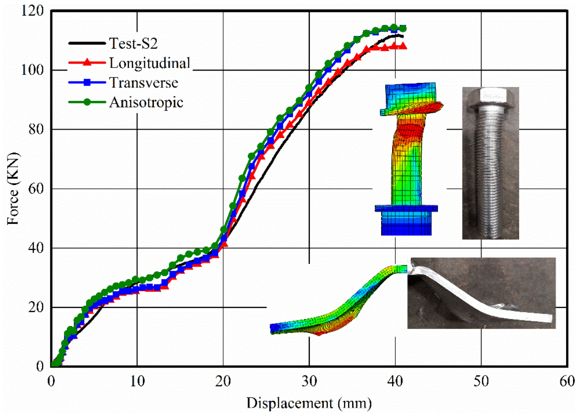

(b) S2

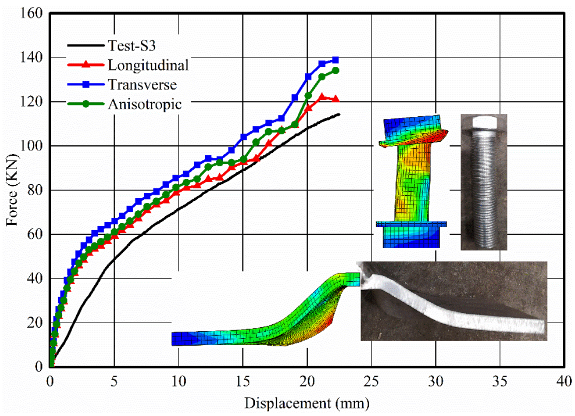

(c) S3

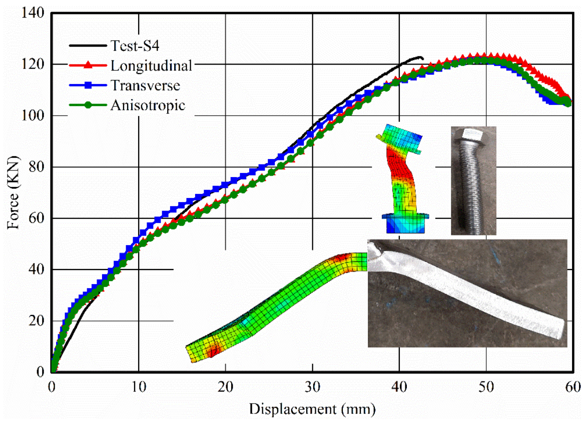

(d) S4

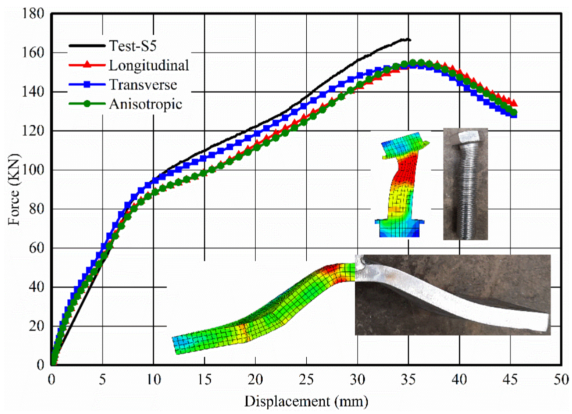

(e) S5

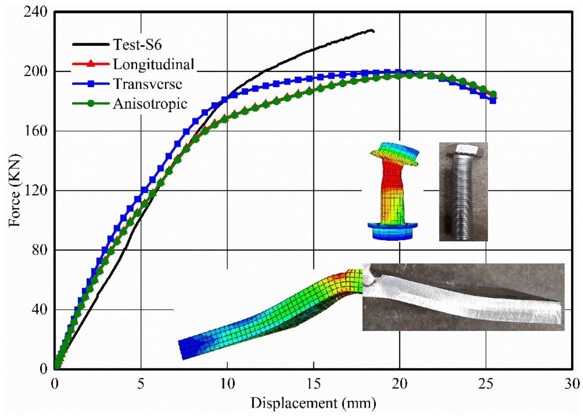

(f) S6

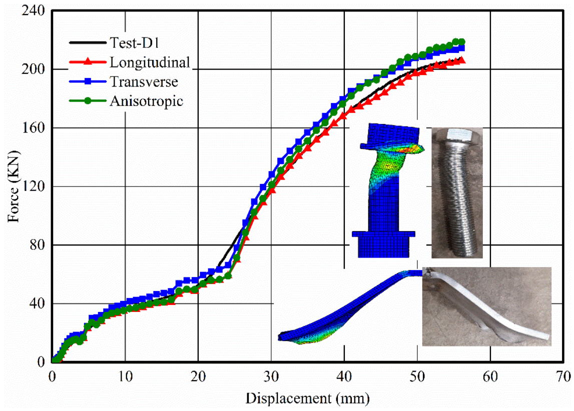

(g) D1

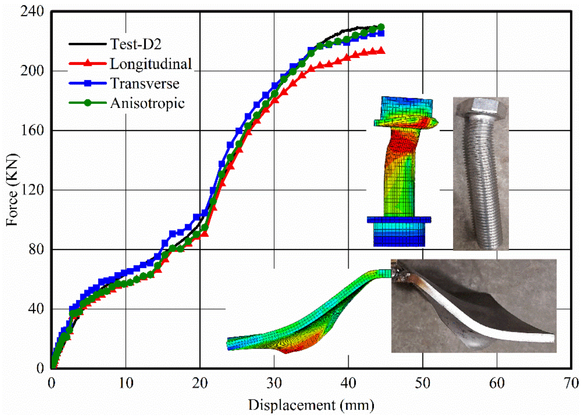

(h) D2

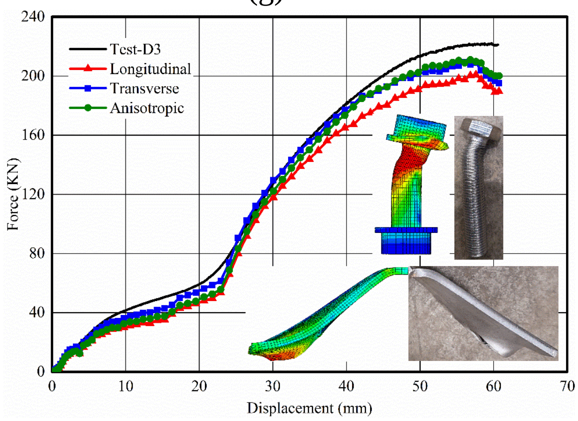

(i) D3

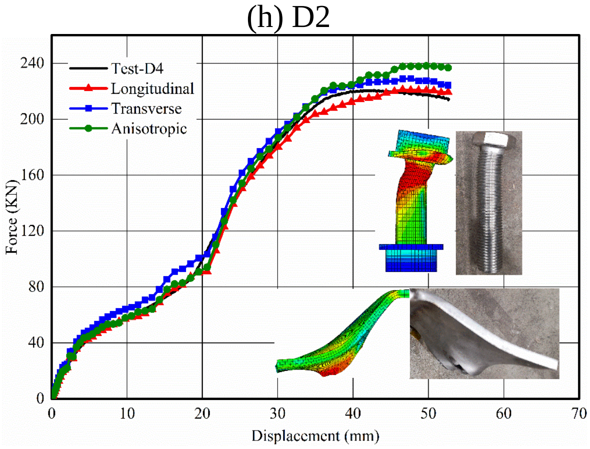

(j) D4

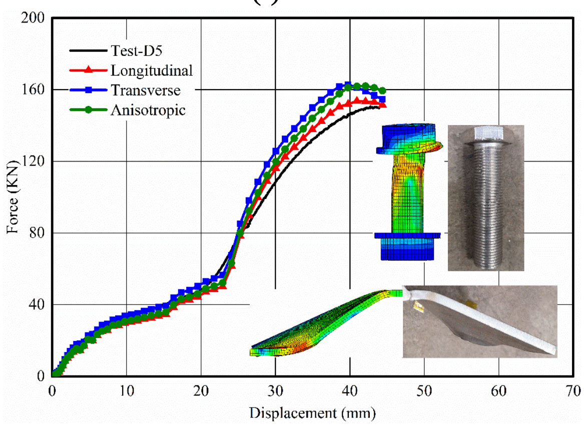

(k) D5

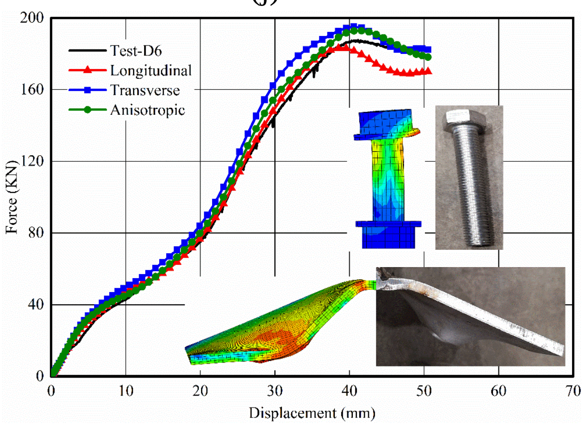

(l) D6

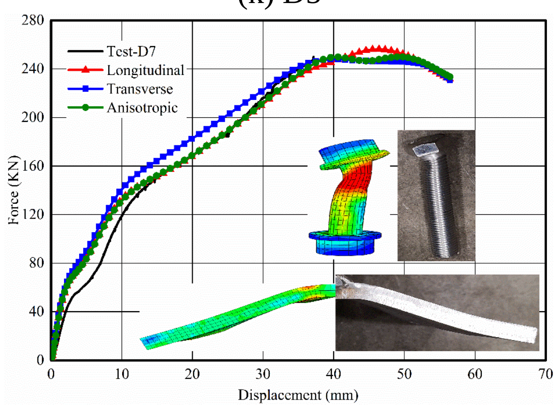

(m) D7

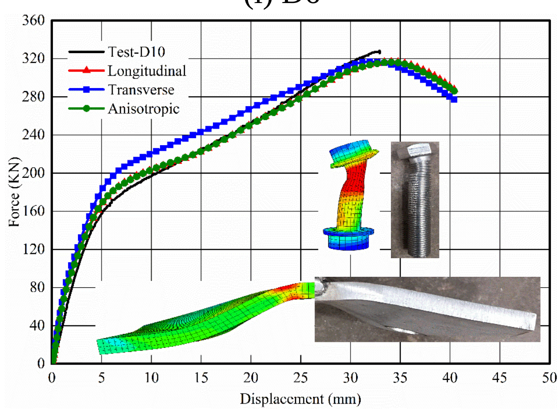

(n) D10

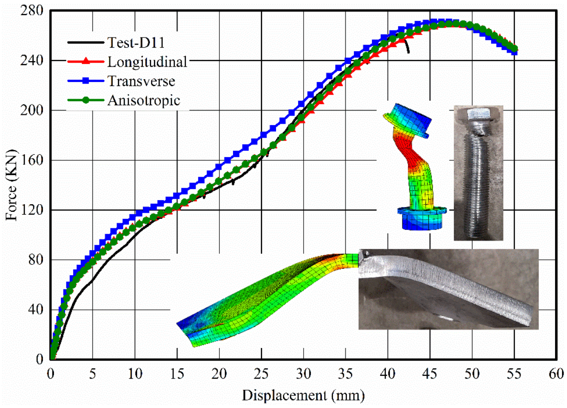

(o) D11

Fig. 5. The force-displacement curves and the failure modes of the specimens. (The colours in the figure represents the von Mises stress.)

The numerically predicted plastic and ultimate resistances F_{pl} and F_u for all T-stubs, as well as the displacement at ultimate resistance Δ_u are reported in Table 3 for all three material modelling assumptions. The ratios of the corresponding numerical over experimental ratios are reported in Table 4. The average values of the numerical over experimental plastic resistance ratios $F_{pl,FE} / F_{pl,Exp}$ are 0.93, 1.05 and 0.96 with coefficients of variation (COV) of 0.07, 0.08 and 0.06 for the FE models assuming isotropic longitudinal, isotropic transverse and anisotropic material response, respectively. In terms of the ultimate load, the corresponding ratios are 0.97, 1.01 and 1.01 with COV of 0.05, 0.08 and 0.08, respectively. The respective mean ratios of the numerical over experimental displacement at ultimate load ratios $\Delta_{u,FE} / \Delta_{u,Exp}$ are 1.05, 1.03 and 1.07 with COV of 0.09, 0.07 and 0.10. The main difference between each curve in Fig. 5 is the plastic resistance values which are given in Table 3 based on considered constitutive models. It was evidenced that considering the longitudinal material response in numerical models provides conservative numerical over experimental plastic resistance ratios, these ratios are obtained more accurately while accounting anisotropic constitutive model in the FE models since the material exhibited a 0.2% proof stress in the transverse direction 21% and 7% higher than that in the longitudinal direction for 5 mm and 10 mm coupons, respectively.

Hence it can be concluded that accounting for material anisotropy when modelling ferritic stainless steel T-stubs is necessary to obtain accurate FE predictions of the structural response. This is expected since in the vicinity of the bolt holes, T-stubs are subjected to a multi-axial stress state hence the behaviour of the material in all directions needs to be considered by the numerical model. If data on material anisotropy are not available, the longitudinal material properties should be adopted to ensure conservative capacity predictions.

Table 3: Experimental and numerical results for plastic resistance, ultimate resistance and displacement at ultimate resistance.

#	Test results			FE results								
				Longitudinal			Transverse			Anisotropic		
	$F_{Pl,Exp}$ (kN)	$F_{u,Exp}$ (kN)	$\Delta_{u,Exp}$ (mm)	$F_{Pl,FE}$ (kN)	$F_{u,FE}$ (kN)	$\Delta_{u,FE}$ (mm)	$F_{Pl,FE}$ (kN)	$F_{u,FE}$ (kN)	$\Delta_{u,FE}$ (mm)	$F_{Pl,FE}$ (kN)	$F_{u,FE}$ (kN)	$\Delta_{u,FE}$ (mm)
S1	16.8	102.1	54.0	14.5	97.1	53.8	16.0	96.3	53.8	15.0	96.3	53.8
S2	22.3	111.8	41.0	20.0	108.0	39.9	21.0	114.1	40.9	23.0	114.1	39.9
S3	47.0	114.3	22.5	46.0	122.0	21.1	53.0	138.9	22.2	47.0	138.9	22.2
S4	48.0	122.7	42.2	45.0	122.8	49.8	51.0	121.6	49.0	47.0	121.5	49.8
S5	93.5	167.0	34.9	81.0	154.2	37.0	88.0	153.5	35.4	82.0	154.9	36.3
S6	188.0	227.7	18.4	166.0	197.8	21.2	184.0	199.4	19.3	167.0	197.3	21.2
D1	31.0	207.5	55.8	29.5	205.7	56.1	33.5	214.4	56.1	30.0	214.4	55.3
D2	46.0	229.9	43.5	40.0	213.3	44.4	49.5	225.4	44.4	44.5	225.4	44.4
D3	37.5	222.1	59.7	31.2	200.9	57.6	34.0	209.2	56.1	32.2	209.2	56.8
D4	40.0	220.8	42.8	37.0	221.2	46.6	46.3	229.0	47.7	39.8	229.0	49.7
D5	29.0	150.5	43.0	27.0	153.6	40.9	32.2	162.8	39.8	28.0	162.8	42.1
D6	36.0	187.5	41.2	33.0	183.1	38.5	41.0	195.1	40.6	36.0	192.8	41.6
D7	127.0	249.9	37.2	128.0	256.2	46.4	136.0	248.0	40.6	127.0	249.9	49.0
D10	170.0	328.1	32.9	178.0	316.7	34.1	198.0	316.9	32.0	177.0	316.2	34.1
D11	92.0	260.9	41.1	93.0	268.7	48.1	98.0	271.2	46.4	92.0	269.6	48.1

Table 4: Numerical over experimental FE results for various material modelling assumptions.

#	Longitudinal			Transverse			Anisotropic		
	$F_{Pl,FE}$ / $F_{Pl,Exp}$	$F_{u,FE}$ / $F_{u,Exp}$	$\Delta_{u,FE}$ / $\Delta_{u,Exp}$	$F_{Pl,FE}$ / $F_{Pl,Exp}$	$F_{u,FE}$ / $F_{u,Exp}$	$\Delta_{u,FE}$ / $\Delta_{u,Exp}$	$F_{Pl,FE}$ / $F_{Pl,Exp}$	$F_{u,FE}$ / $F_{u,Exp}$	$\Delta_{u,FE}$ / $\Delta_{u,Exp}$
S1	0.86	0.95	1.00	0.95	0.94	1.00	0.89	0.94	1.00
S2	0.89	0.96	0.97	0.94	1.02	1.00	1.03	1.02	0.97
S3	0.98	1.06	0.93	1.12	1.22	0.99	1.00	1.22	0.99
S4	0.93	1.00	1.18	1.06	0.99	1.16	0.98	0.99	1.18
S5	0.87	0.93	1.06	0.94	0.92	1.02	0.88	0.93	1.04
S6	0.88	0.87	1.15	0.98	0.88	1.05	0.88	0.87	1.15
D1	0.95	0.99	1.01	1.08	1.03	1.01	0.97	1.03	0.99
D2	0.87	0.93	1.02	1.08	0.98	1.02	0.97	0.98	1.02
D3	0.83	0.90	0.96	0.91	0.94	0.94	0.86	0.94	0.95
D4	0.93	1.00	1.09	1.16	1.04	1.11	0.99	1.04	1.16
D5	0.93	1.02	0.95	1.11	1.09	0.93	0.96	1.09	0.98
D6	0.92	0.98	0.93	1.14	1.04	0.99	1.00	1.03	1.01

D7	1.01	1.02	1.25	1.08	0.99	1.09	1.00	1.00	1.32
D10	1.04	0.96	1.04	1.16	0.96	0.97	1.04	0.96	1.04
D11	1.01	1.03	1.18	1.06	1.04	1.12	1.00	1.03	1.18
Average	0.93	0.97	1.05	1.05	1.01	1.03	0.96	1.01	1.07
COV	0.07	0.05	0.09	0.08	0.08	0.07	0.06	0.08	0.10

In addition, in all cases, the T-stubs failed in mode 1 with the formation of 4 yield lines and significant plastic deformation. In the failure modes shown in Fig. 5, the flexural deformations of the flanges are not pronounced since the photos were taken at the end of the test and the membrane action developed in the T-stub flanges dominates the observed plastic deformation. A close-up of the failure modes of specimens S1, D3, D5, D6 and D11 are shown in Fig. 6 where the numerically obtained equivalent plastic strain at the end of the analysis is also depicted for these specimens. The specimen S1 ultimately failed by bearing of the T-stub flange plate since at high deformations the bolts anchoring the membrane action of the T-stub flanges were subjected to high levels of shear forces. In specimen D3, the initiation of a crack is clearly seen at the bolt hole due to high levels of plastic strain, whilst D5 and D6 ultimately failed by fracture of the flange in-between the bolts due to the strain concentration between the bolt holes. Specimen D11 failed by the fracture of the bolts and the strain concentration of the bolts in the FE model agree well with the tested T-stub. All these failure types were accurately predicted by the developed FE models where the locations of accumulation of plastic strain coincides with the location where the cracks were observed during the tests.

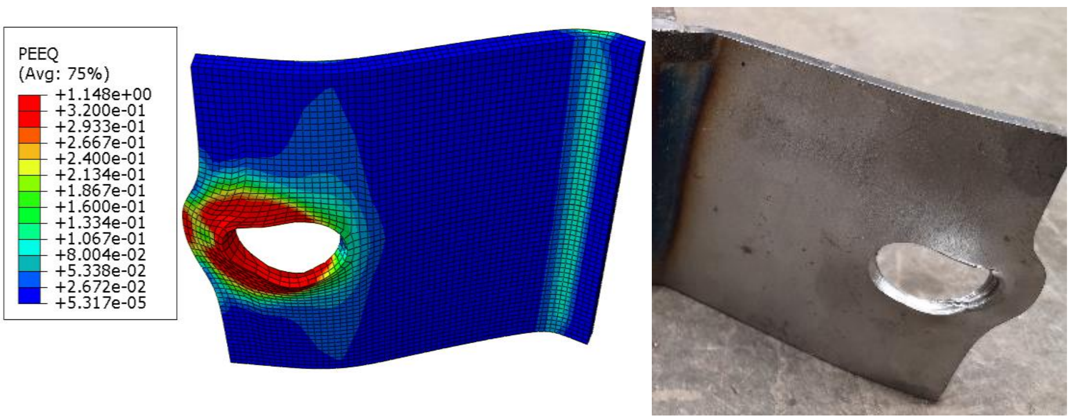

a) S1

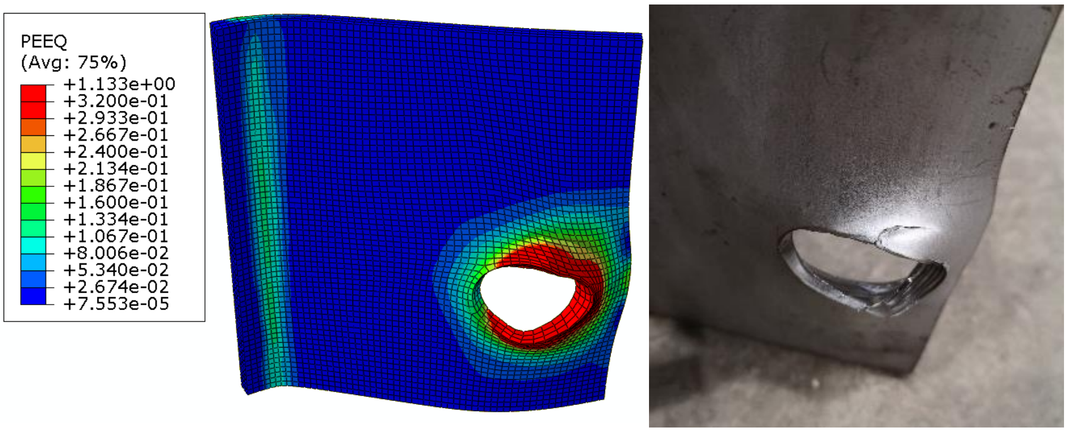
PEEQ
(Avg: 75%)
+1.133e+00
+3.200e-01
+2.933e-01
+2.667e-01
+2.400e-01
+2.134e-01
+1.867e-01
+1.600e-01
+1.334e-01
+1.067e-01
+8.006e-02
+5.340e-02
+2.674e-02
+7.553e-05

b) D3

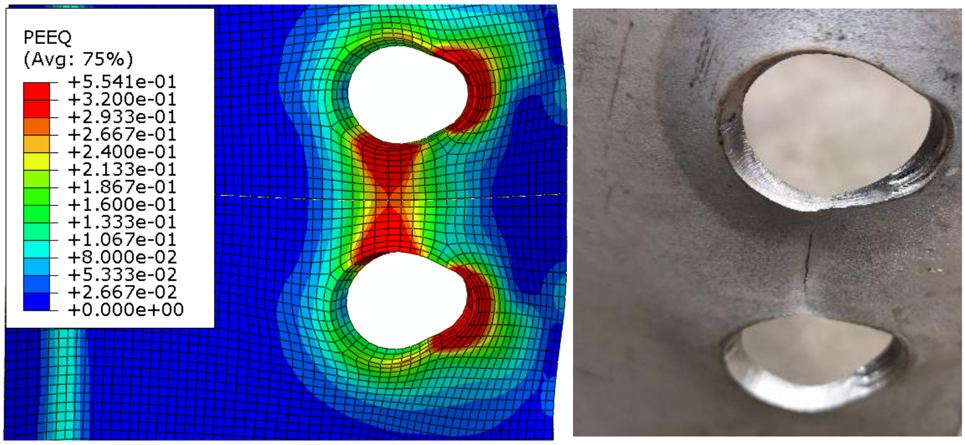
PEEQ
(Avg: 75%)
+5.541e-01
+3.200e-01
+2.933e-01
+2.667e-01
+2.400e-01
+2.133e-01
+1.867e-01
+1.600e-01
+1.333e-01
+1.067e-01
+8.000e-02
+5.333e-02
+2.667e-02
+0.000e+00

c) D5

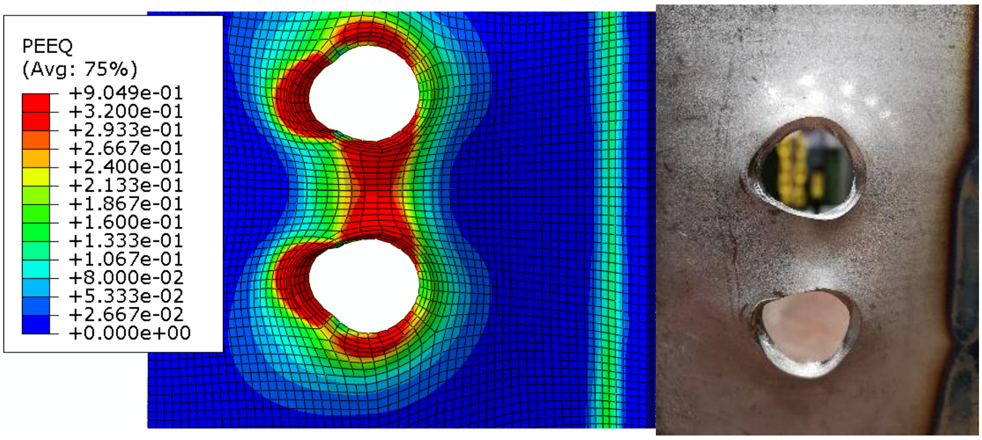
PEEQ
(Avg: 75%)
+9.049e-01
+3.200e-01
+2.933e-01
+2.667e-01
+2.400e-01
+2.133e-01
+1.867e-01
+1.600e-01
+1.333e-01
+1.067e-01
+8.000e-02
+5.333e-02
+2.667e-02
+0.000e+00

d) D6

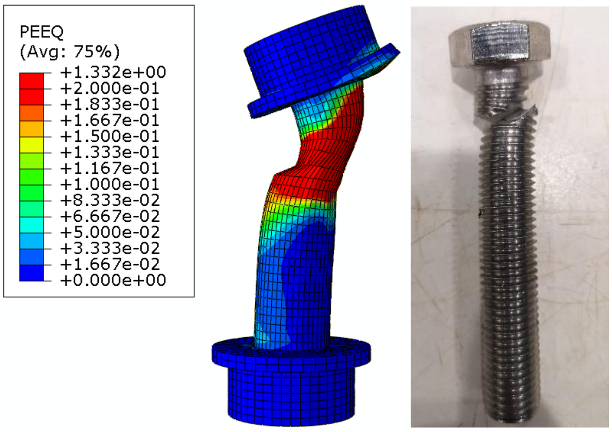

e) D11

Fig. 6. Experimental and numerical failure modes of a) S1, b) D3, c) D5, d) D6 and e) D11.

3.2. Stress distribution through the flange thickness

Having demonstrated the ability of the FE models to replicate the experimentally observed response, the validated models are utilised to extract valuable information regarding the stress distribution through the flange thickness at specific load levels. In Fig. 7, the stress distribution through the flange thickness is reported at three sections along the length of the T-stubs, at the end of the fillet weld as shown in the relevant figures. The selected locations include the middle of the T-stub, the end of the T-stub and the location of the bolt. The reported normal stresses are oriented perpendicular to the web, have been normalised by the longitudinal $\sigma_{0.2}$ and are plotted on the x-axis, whilst the through thickness locations at which they occur are on the y-axis. For each of the three locations along the length of the T-stub sections where the stress values are reported, two load levels are considered, namely the load corresponding to the plastic resistance of the T-stub $F_{pl,FE}$ and the ultimate load $F_{u,FE}$ with the stress distribution curves are denoted with solid and dotted lines, respectively. It should be noted that to obtain local stress values with a sufficient accuracy, the models from which the stress distributions were extracted employed 4 elements through the thickness, despite, as earlier stated, three elements through the thickness suffice to obtain an accurate prediction of the global response of the T-stubs. EN

1993-1-8 [1] assumes rigid plastic material response of the flanges of the T-stub and the derivation of the mode 1 plastic resistance load is based on rigid plastic analysis. For materials with a well-defined yield plateau such as carbon steel such an assumption is reasonable, whilst for stainless steels, which exhibit a gradual loss of stiffness and significant strain-hardening the validity of this assumption is questionable. Hence it is of interest to determine the actual stress distribution through the T-stub thickness at the load level consistent with the plastic resistance of the T-stub.

In Fig. 7, for all models, it can be observed that at the attainment of F_{pl} the stress distributions in all locations are symmetric with equal and opposite stress values occurring at the top and bottom nodes of the T-stubs, thus confirming that the main load carrying mechanism up to the attainment of the plastic resistance of the section is bending. In all models, the T-stub section at the bolt location experiences higher stress values (red curves) compared to the other sections, whilst the lowest stress values are observed at the free ends of the T-stubs (green curves) with the intermediate locations (blue curves) being in-between depending on the bolt arrangement. In models with large distances between the bolt axis and the T-stub web (large m values) like the models for specimens D3 and D5, the edge of the T-stub experiences significantly lower stresses, which are predominantly elastic, whilst at the same load level the sections at the bolt axis are subjected to inelastic stresses at or above the nominal yield stress. For models D2 and D4 a more uniform stress distribution at the plastic load level can be observed along the T-stubs. For all models, at the attainment of the plastic resistance of the T-stub, the maximum recorded stress is approximately 25% higher than the nominal yield stress, a value that corresponds to the ultimate tensile stress in the longitudinal direction as reported in [35]. In a recent study on austenitic and duplex stainless steel T-stubs [33] the respective value was 100% higher than the nominal yield stress, due to the significantly more favourable strain-hardening characteristics that these grades exhibit compared to ferritic stainless steel.

An interesting observation can be made with regards to the stress distribution at the ultimate load (dotted curves in Fig. 7). In all cases the dotted lines shift to the right and a clear asymmetry emerges; the T-stubs are no longer working predominantly in flexure; they are carrying simultaneously bending moment and tension due to membrane action. Hence the neutral axis of the sections can be seen to have moved towards the bottom (compression side) of the T-stub. This observation confirms the change of the load transfer mechanism form flexural to membrane at high deformations.

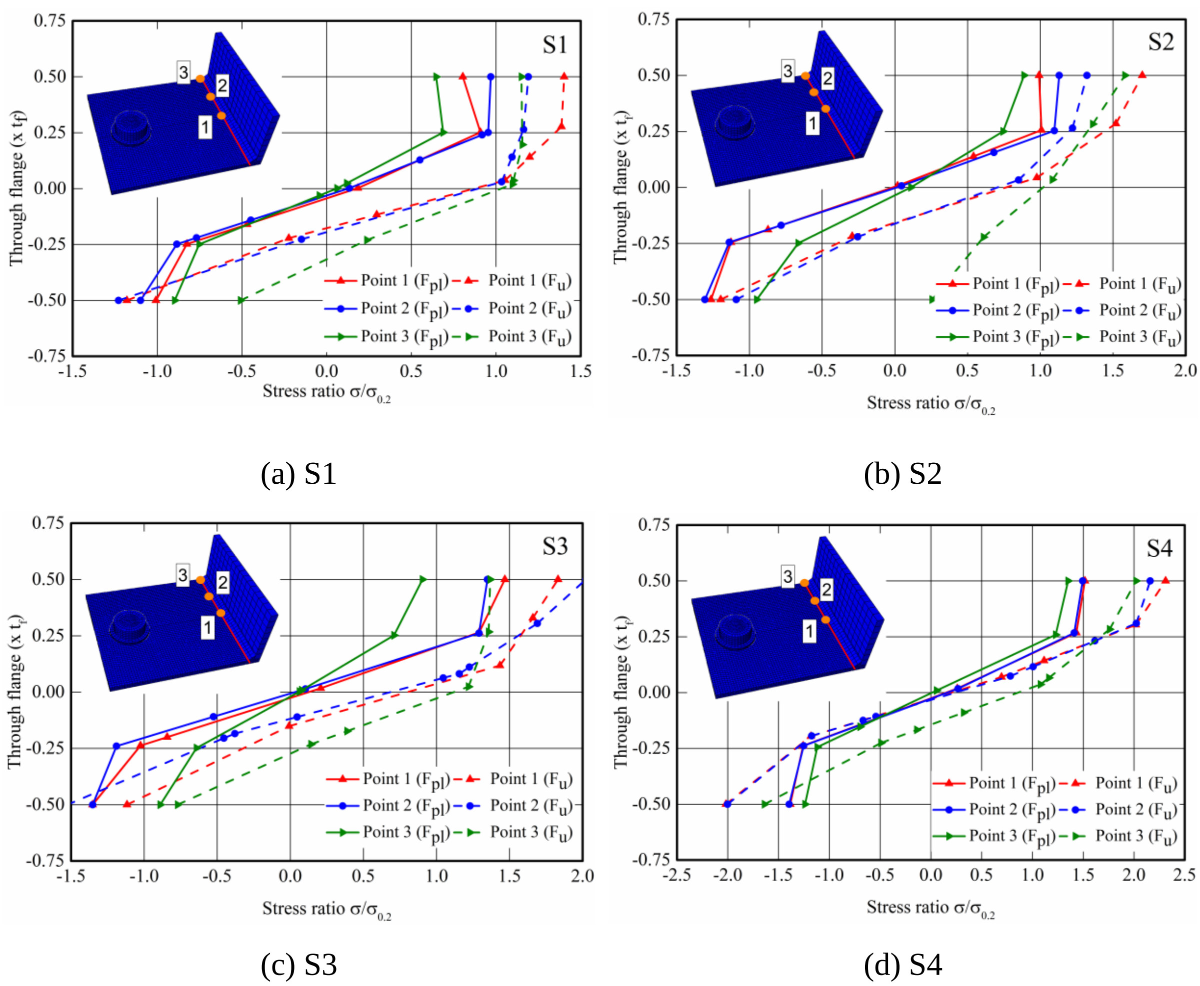

(a) S1

(b) S2

(c) S3

(d) S4

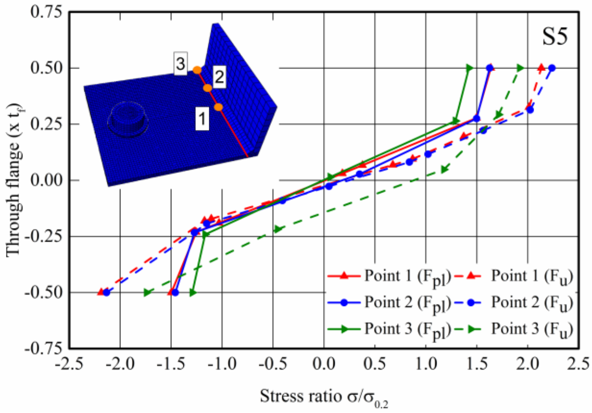

(e) S5

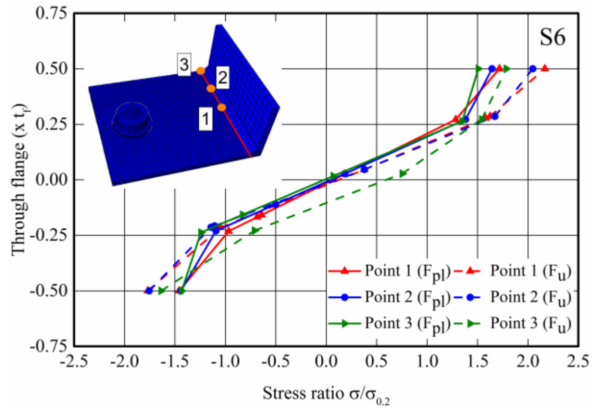

(f) S6

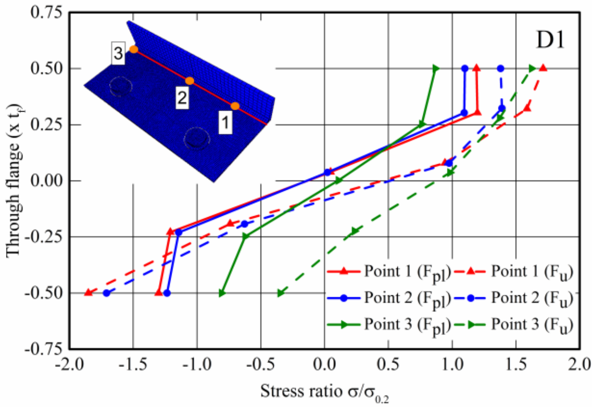

(g) D1

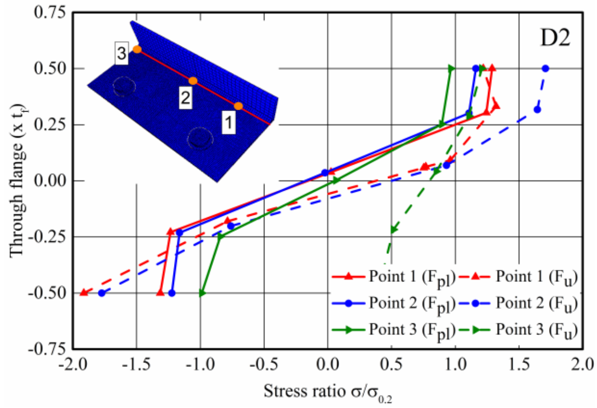

(h) D2

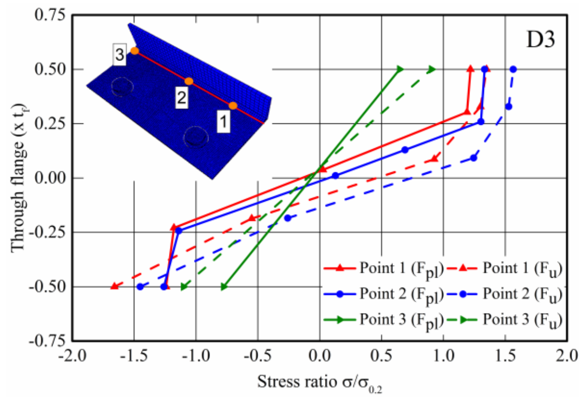

(i) D3

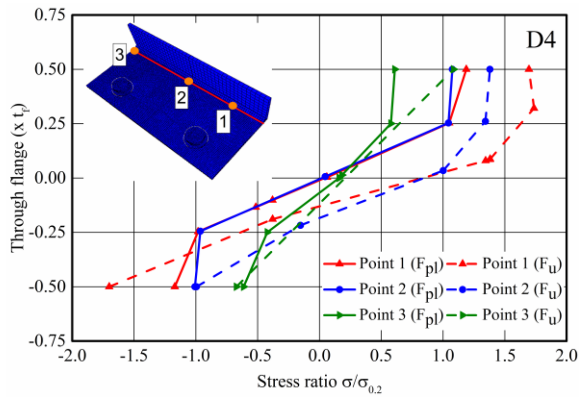

(j) D4

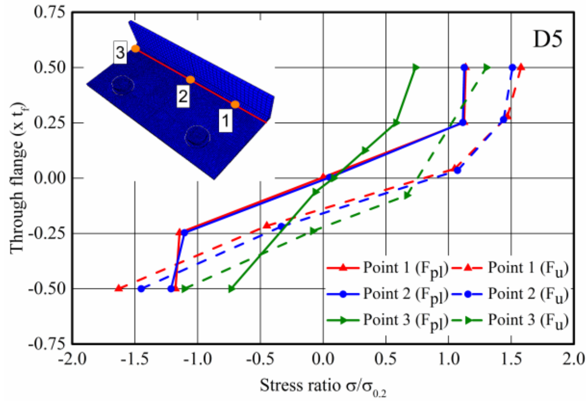

(k) D5

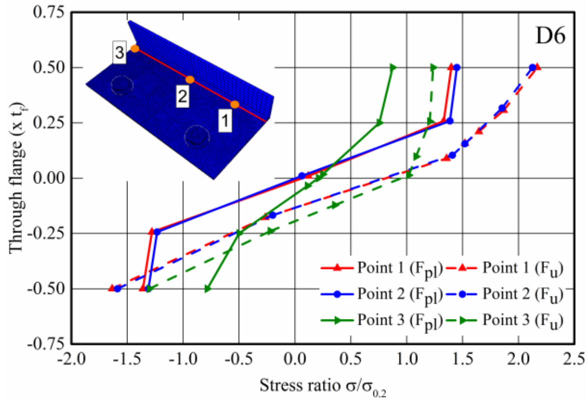

(l) D6

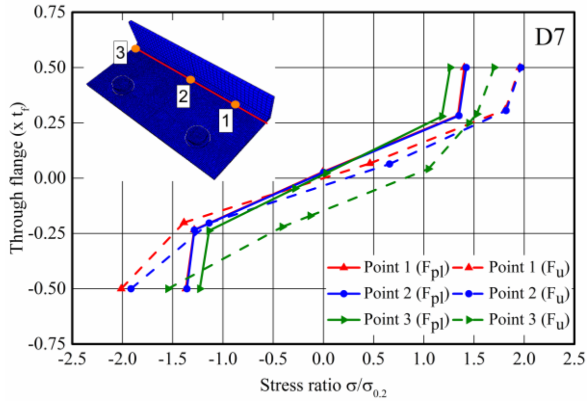

(m) D7

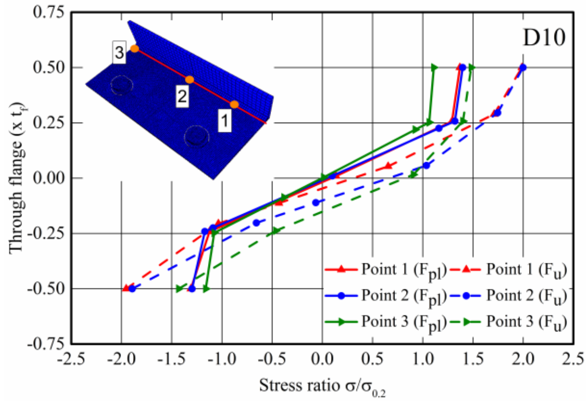

(n) D10

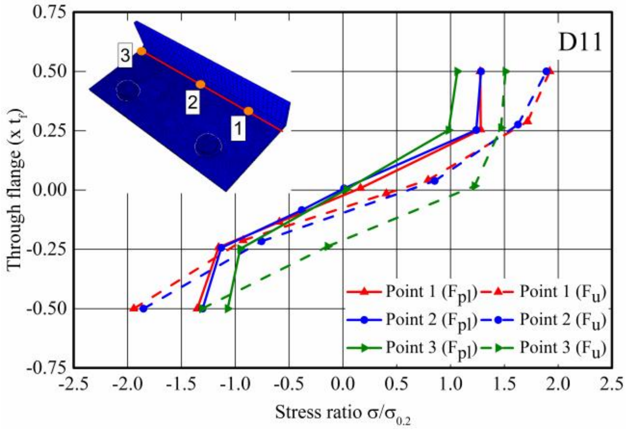

(o) D11

Fig. 7. The stress distribution through the flange plate thickness.

3.3. Results of incorporating the bolt fracture

Bolt fracture was included to the FE modelling of S4, S5, D7, D10 and D11 which exhibited severe damage of the bolts using the ductile damage model in ABAQUS. The plastic strain at damage initiation was defined as a function of stress triaxiality according to Eq. (1), whilst no damage evolution was considered. Hence the time increament at which the damage initiation criterion was fulfilled was obtained and at this time increament the force-displacement curves truncated, as evidenced by the suddent drop exhibited by the red curves in Fig. 8. This approach eliminates the need for explicit fracture modelling and allows the experimental curves (incoporating damage) to be compared to a modelling approach effectively assuming instantaneous fracture (red curves in Fig. 8). The force-displacement curves of the numerical models are presented in Fig. 8, with the blue lines not accounting for bolt fracture and the red ones corresponding to instant fracture when the relevant plastic strain is reached. The results show that the assumption of instant fracture yields conservative results and the final part of the tested curves can not be captured accurately, whilst not considering bolt fracture (blue lines) over estimates the deformations that the specimens can reach and hence the ductility. Hence, the necessity of including damage propogation into the FE model to obtain the load and displacement at failure is highlighted, whilst for design purposes, where a reasonable level of conservatism is necessary, assuming instant fracture is warranted.

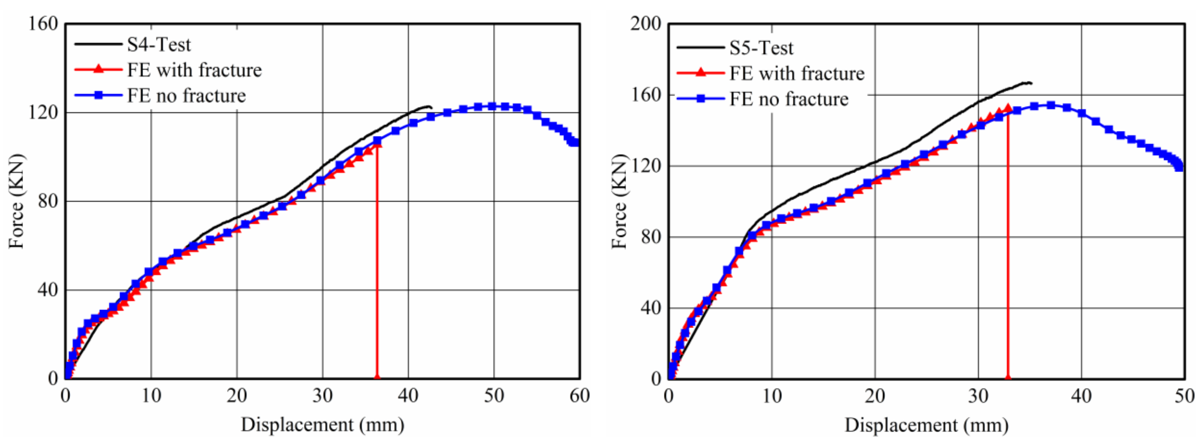

(a) S4 (b) S5

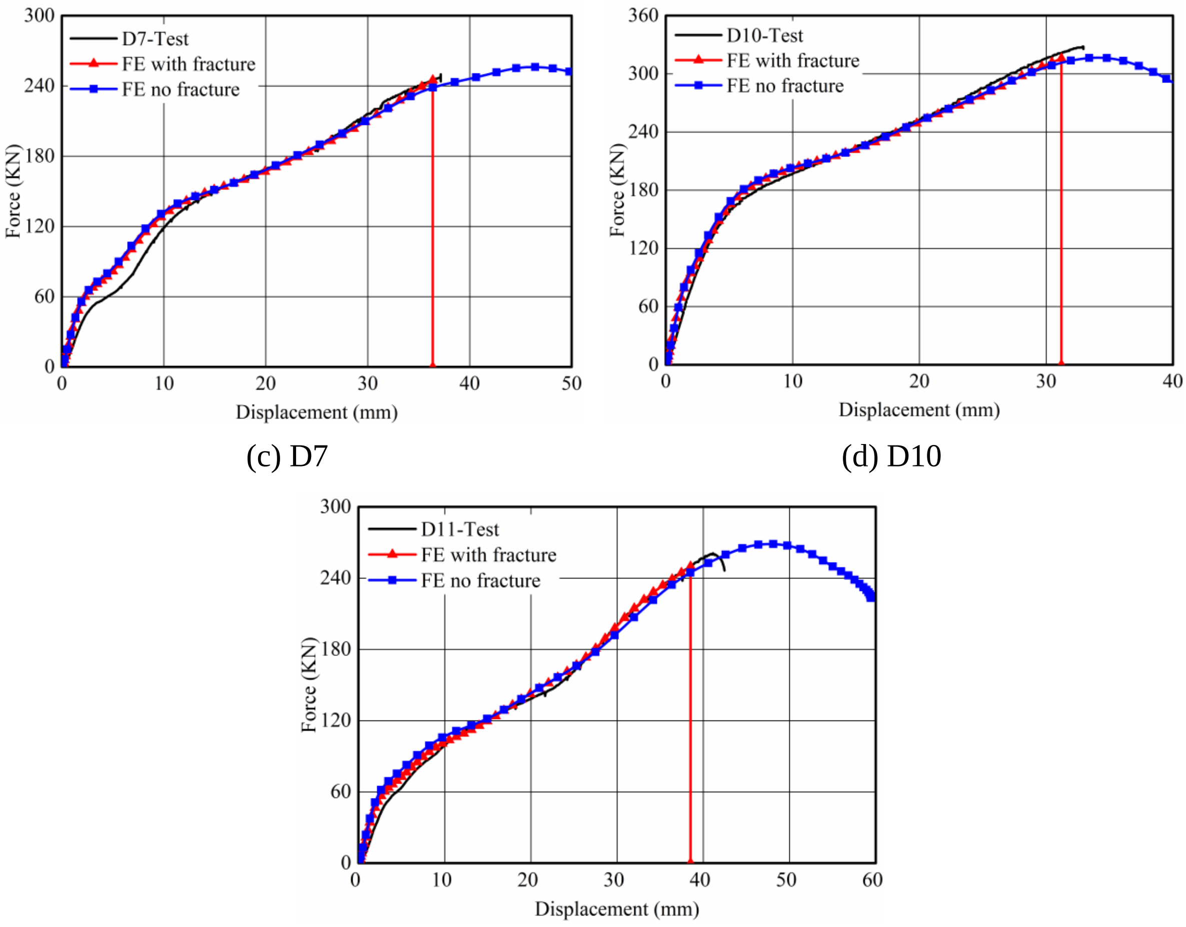

(c) D7 (d) D10

(e) D11

Fig. 8. The force-displacement curves of FE models with proposed damage model.

4. Parametric study

A comprehensive parametric study has been conducted in the scope of this study with the aim of quantifying membrane effects and assessing the applicability of relevant predictive equations as discussed in section 5. The modelling assumptions for the parametric analysis follow the ones discussed previously in the validation of the numerical models in section 2.1. The parametric studies consider bolted T-stub specimens with a single bolt row only.

4.1. FE modelling and assumptions

The FE model for the parametric study of ferritic stainless steel bolted T-stubs is constructed based on section 2. The dynamic explicit solver was utilized and boundary conditions and loading mechanism remained unchanged. A total of 35 FE models which were created based on the selected parameters in Table 5 were performed. The material properties reported in Table 1 for 5 mm thick ferritic stainless steel plates are utilised in the FE model. The predicted plastic and ultimate resistances and corresponding displacements are reported in Table 6.

Table 5: Geometric dimensions of the specimens for the parametric study (units are in mm).

Material	Bolt	$t_f = t_w$	Width	m	n	d_b	h_f
Ferritic	A4-80	3	$b_f = 220$	25	75	16	6
		6		30	70		
		9		40	60		
		12		50	50		
		15		60	40		
				70	30		
				75	25		

5. Design recommendations

5.1. EN 1993-1-8 design provisions for the plastic resistance F_{pl}

The expressions to predict the plastic resistances corresponding to the three failure modes identified in EN 1993-1-8 [1] for stainless steel bolted T-stubs are given by Eqs. 2-4, where all symbols are defined in EN 1993-1-8 [1].

Type-1 $$F_{1,Rd} = \frac{(8n - 2e_w)M_{f,1,Rd}}{2mn - e_w(m+n)} \quad (2)$$

Type-2 $$F_{2,Rd} = \frac{2M_{f,2,Rd} + n\Sigma F_{t,Rd}}{m+n} \quad (3)$$

Type-3 $$F_{3,Rd} = \Sigma F_{t,Rd} \quad (4)$$

Furthermore, the theoretical relationship between the thickness squared (t_f^2) and plastic resistance of T-stubs is depicted in Fig. 9. It can be observed that the resistance F_{pl} is proportional to t_f^2 for type 1 and type 2 failure modes, albeit with a different factor of proportionality, however type-3 failure mechanism is not affected by any change in thickness since it only involves bolt failure.

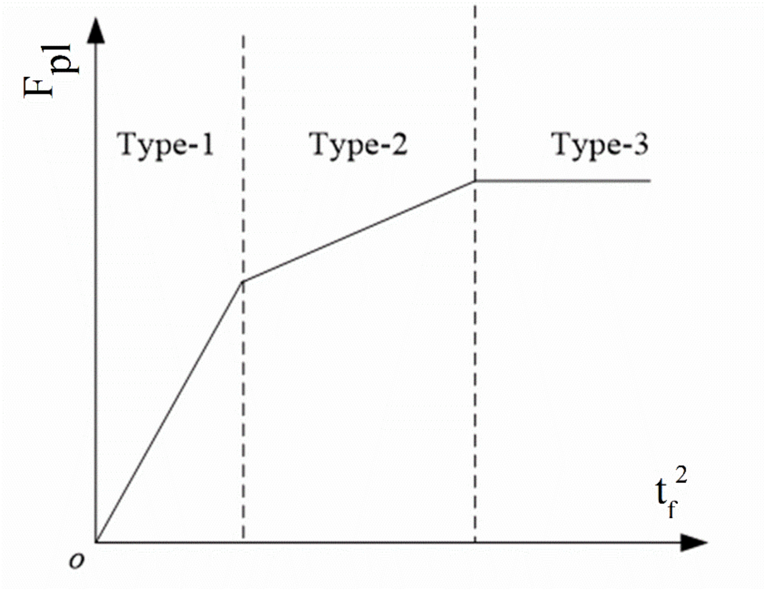

Fig. 9. Theoretical relationship between F_{pl} and t_f^2 provided in EN 1993-1-8 [1].

The parametric study results are considered to assess the EN 1993-1-8 [1] in terms of plastic resistance predictions. In Table 6, the ratio of the plastic resistance predicted based on EN 1993-1-8 [1] over the numerical one is reported. The average ratio was 0.90 with a standard deviation of 0.08. It was concluded that the plastic resistance predictions based on EN 1993-1-8 [1] provided good estimations for ferritic stainless steel bolted T-stubs failing in either mode 1 or mode 2. Since the strain-hardening characteristics of ferritic stainless steels is similar to that of carbon steel, the predictions for plastic resistance of the ferritic T-stubs were obtained in a good agreement with the parametric analysis results. Similar conclusions were reported by Yapici et al. [35] regarding the plastic resistance predictions of ferritic stainless steel T-stubs by EN 1993-1-8 [1] using experimental results.

Table 6. Assessment of EN 1993-1-8 based on the parametric study.

#	Material	n	t_f	m	b_{eff}	b_f	$F_{pl, FE}$	$\Delta_{pl, FE}$	$F_{u, FE}$	$\Delta_{u, FE}$	Failure mode	$F_{pl,EC3}$/ $F_{pl,FE}$
1	Ferritic	75	3	25	100	220	23.5	0.6	74.1	53.1	Mode 1	0.66
2	Ferritic	70	3	30	100	220	15.0	0.8	75.8	66.2	Mode 1	0.83
3	Ferritic	60	3	40	100	220	10.9	1.2	85.2	98.5	Mode 1	0.81
4	Ferritic	50	3	50	100	220	10.0	2.0	76.6	72.5	Mode 1	0.69
5	Ferritic	40	3	60	100	220	5.8	1.3	76.5	98.5	Mode 1	0.98
6	Ferritic	30	3	70	100	220	5.3	1.6	65.6	79.0	Mode 1	0.93

7	Ferritic	25	3	75	100	220	5.9	3.8	56.0	63.0	Mode 1	0.79
8	Ferritic	75	6	25	100	220	78.0	0.6	158.4	28.9	Mode 1	0.80
9	Ferritic	70	6	30	100	220	52.2	0.7	153.7	30.5	Mode 1	0.95
10	Ferritic	60	6	40	100	220	37.4	0.9	147.1	42.9	Mode 1	0.94
11	Ferritic	50	6	50	100	220	33.5	1.0	132.9	41.2	Mode 1	0.82
12	Ferritic	40	6	60	100	220	23.5	1.3	124.2	44.3	Mode 1	0.97
13	Ferritic	30	6	70	100	220	20.8	1.5	117.7	48.0	Mode 1	0.95
14	Ferritic	25	6	75	100	220	20.5	1.8	121.2	78.0	Mode 1	0.91
15	Ferritic	75	9	25	100	220	155.0	0.5	193.9	15.3	Mode 1	0.91
16	Ferritic	70	9	30	100	220	118.4	0.9	183.9	20.1	Mode 1	0.94
17	Ferritic	60	9	40	100	220	84.6	1.0	165.2	26.4	Mode 1	0.93
18	Ferritic	50	9	50	100	220	77.0	1.0	147.2	31.5	Mode 1	0.80
19	Ferritic	40	9	60	100	220	55.0	1.1	133.9	34.6	Mode 1	0.93
20	Ferritic	30	9	70	100	220	48.0	1.3	116.6	37.4	Mode 1	0.93
21	Ferritic	25	9	75	100	220	48.0	1.3	111.2	37.9	Mode 1	0.88
22	Ferritic	75	12	25	100	220	195.0	0.7	205.2	7.7	Mode 2	0.87
23	Ferritic	70	12	30	100	220	170.5	0.9	197.0	9.5	Mode 2	0.95
24	Ferritic	60	12	40	100	220	146.3	1.1	178.0	14.4	Mode 1	0.96
25	Ferritic	50	12	50	100	220	134.0	1.1	159.6	19.9	Mode 1	0.82
26	Ferritic	40	12	60	100	220	101.0	1.4	141.3	25.1	Mode 1	0.90
27	Ferritic	30	12	70	100	220	85.2	1.8	121.6	29.1	Mode 1	0.93
28	Ferritic	25	12	75	100	220	87.0	1.9	117.5	35.7	Mode 1	0.86
29	Ferritic	75	15	25	100	220	208.0	0.7	225.9	7.8	Mode 2	0.93
30	Ferritic	70	15	30	100	220	192.0	0.8	216.8	9.5	Mode 2	0.95
31	Ferritic	60	15	40	100	220	182.0	0.9	199.5	11.3	Mode 2	0.92
32	Ferritic	50	15	50	100	220	154.2	1.0	176.0	14.4	Mode 2	0.98
33	Ferritic	40	15	60	100	220	132.4	1.2	157.4	17.7	Mode 2	0.97
34	Ferritic	30	15	70	100	220	108.6	1.4	139.1	25.1	Mode 2	0.97
35	Ferritic	25	15	75	100	220	98.7	1.4	139.2	41.6	Mode 2	0.96
											Average	0.90
											St. dev	0.08

Furthermore, the numerically obtained plastic force F_{pl} is plotted against the square of the flange thickness t_f^2 for each model of the parametric study in Fig. 10. It can be concluded that the predicted failure modes based on EN 1993-1-8 [1] agree well with the plastic force versus t_f^2 behaviours. The curves corresponding to an *m* value between 40 and 75 mm are almost linear with respect to the thickness squared until the flange thickness is reached to 12 mm. While the flange thickness becomes 15 mm, a second linear branch emerges in the curves. This is attributed to the change in the failure modes of all specimens with 15 mm flange thickness (specimens 31-35 in Table 6) based on EN 1993-1-8 [1] in Table 6. Additionally, a second linear branch are observed for the curves with an *m* distance of 30 and 35 mm when the thickness is 12 mm which means that the change in failure mode becomes earlier for the T-stubs with lesser m distances. The change in the failure mode of specimens 22 and 23 in the parametric study was well represented by the plastic force versus t_f^2 curves given in Fig. 10. The change in the slope of the curves corresponds to the change of the failure mode predictions based on EN 1993-1-8 [1] from mode 1 to mode 2, the predicted failure modes of the specimens.

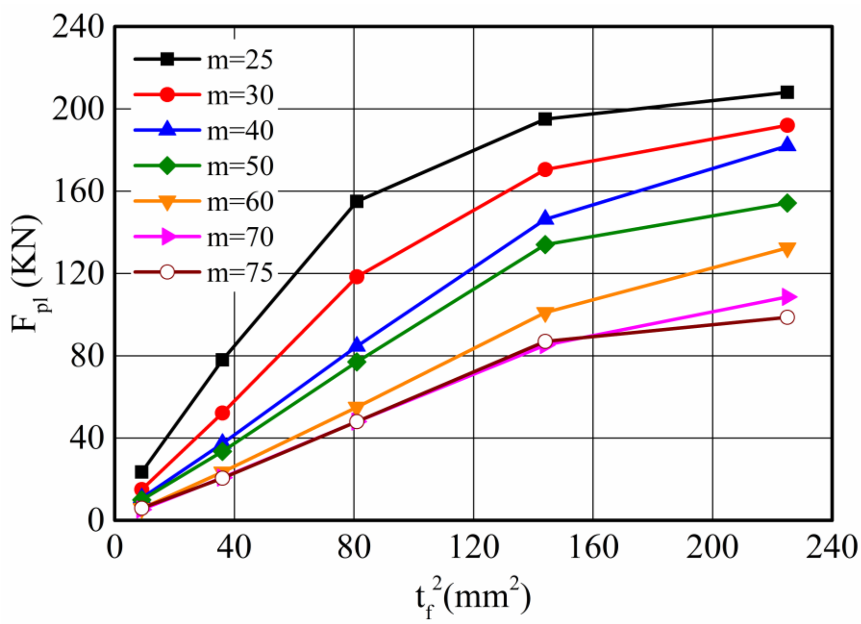

Fig. 10. Relationships between F_{pl} and t_f^2 for the parametric study.

5.2. Prediction of ultimate resistance force F_u

Predictive equations for the determination of the ultimate force of a T-stub were recently proposed by Tartaglia et al. [48] for carbon steel specimens. Its applicability to stainless steel T-stubs is assessed herein based on the reported experimental and numerical results. The proposed predictive equations are given by Eqs. 5-7 where $F_{T,1}$ and $F_{T,2}$ are the resistances for failure mode 1 and 2 according to EN 1993-1-8 [1], whilst $F_{T,LD}$ is an additional force due to the development of membrane action at large deformations. The l_{eff} is the effective length of the T-stub, t_f is the flange thickness, f_u is the ultimate strength of the flange material, $F_{B,R}$ is the bearing resistance calculated based on EN 1993-1-8 [1]. The ratio between the imposed gap opening δ and the distance m is termed as α (Fig. 11) and ψ is a reduction factor applied to the bolts, which accounts for their reduced tensile strength due to the simultaneous presence of shear force and bending moment.

$$F_T=F_{T,1}+F_{T,LD} \text{ for Mode 1} \tag{5}$$

$$F_T=F_{T,2}+F_{T,LD} \text{ for Mode 2} \tag{6}$$

$$F_{T,\,LD}=2\times\min\left(\frac{l_{eff}}{2}\times t_f\times f_u\times \sin\alpha;\, F_{B,\,R}\times \tan\alpha\,;F_{t,\,R}\times\psi\right) \tag{7}$$

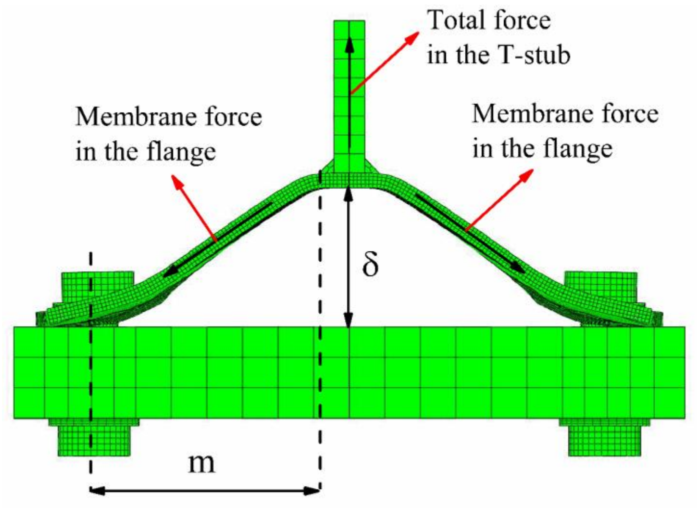

Fig. 11. Development of membrane forces in bolted T-stubs.

5.2.1. Assessment of predictive equations using experimental results in the literature

The experimental test results on austenitic and duplex stainless steel bolted T-stubs under monotonic loading reported by Yuan et al. [20,33] were used to validate the design formula proposed by Tartaglia et al. [48] to predict the ultimate resistances. A total of 27 bolted T-stubs were considered with three different geometric configuration such as single and double bolt rows named as S and D, respectively. The experimental plastic and ultimate forces and predicted ultimate forces are represented in Table 7 with comparisons. The parameter β in Table 7 is defined as the ratio of plastic resistance of the T-stub for mode 1 failure over the resistance of the bolts [35]. The proposed expressions in Eqs. 5-7 by Tartaglia et al. [48] provide accurate ultimate resistance predictions for austenitic and duplex stainless steel bolted T-stubs. The average ratio of predicted and experimental ultimate force is 0.97 with a standard deviation of 0.11.

Table 7: Assessment of proposed design formula by Tartaglia et al. [48] using available test data for austenitic and duplex stainless steel T-stubs.

#	Material	$F_{pl,Exp.}$	$F_{u,\ Exp.}$	β	$F_{T,pred.}$	$F_{T,pred}$ / $F_{u,Exp.}$
S1	EN 1.4301	154.0	200.2	0.48	183.0	0.91
S2	EN 1.4301	85.8	106.8	0.60	112.4	1.05
S3	EN 1.4462	175.7	198.4	0.58	228.8	1.15
S4	EN 1.4462	93.9	108.9	0.61	124.5	1.14
S5	EN 1.4462	87.6	161.6	0.25	150.9	0.93
S6	EN 1.4301	61.8	104.3	0.34	92.1	0.88
S7	EN 1.4462	105.8	175.2	0.33	172.0	0.98
S8	EN 1.4301	131.2	188.0	0.36	157.8	0.84
S9	EN 1.4301	83.3	108.9	0.60	112.5	1.03
S10s	EN 1.4301	51.2	97.3	0.29	74.8	0.77
S11s	EN 1.4301	43.1	136.1	0.11	114.8	0.84
S12s	EN 1.4462	97.3	111.8	0.96	114.5	1.02
S13s	EN 1.4462	79.6	141.8	0.29	142.4	1.00
S14s	EN 1.4462	127.8	140.0	1.65	142.7	1.02
D1	EN 1.4301	211.1	367.5	0.30	286.2	0.78
D2	EN 1.4301	142.2	179.1	0.37	194.7	1.09
D3	EN 1.4462	97.8	260.9	0.18	234.7	0.90
D4	EN 1.4462	254.1	312.5	0.43	344.5	1.10
D5	EN 1.4462	338.7	382.5	0.56	402.5	1.05
D6	EN 1.4301	150.8	306.6	0.20	277.0	0.90
D7	EN 1.4301	104.4	174.3	0.27	167.6	0.96
D8	EN 1.4301	136.2	181.6	0.37	194.3	1.07
D9s	EN 1.4301	63.3	163.1	0.18	123.6	0.76
D10s	EN 1.4301	50.5	224.3	0.06	208.7	0.93
D11s	EN 1.4462	146.8	182.3	0.58	203.3	1.12
D12s	EN 1.4462	244.7	368.4	0.36	358.2	0.97
D13s	EN 1.4462	131.3	194.6	0.38	196.5	1.01
					Average	0.97
					St. dev.	0.11

5.2.2. Assessment of predictive equations using the parametric study results

The equations proposed by Tartaglia et al. [48] was applied to the ferritic stainless steel bolted T-stubs considering a wide range of parameters and failure modes to predict the ultimate resistances. In Table 8, the summary of the numerical and predicted ultimate resistance forces are reported with the comparison ratios. The average ratio of the ultimate force predicted by the proposed formula over obtained by the numerical parametric analysis is 1.03 with a standard deviation of 0.20 which indicates a slight overprediction of ultimate resistances of FE models. The predictions agree well with the FE models overall for ferritic stainless steel.

Table 8: Assessment of proposed design formula by Tartaglia et al. [48] using the parametric study results.

#	Material	n	t_f	m	b_{eff}	b_f	F_u	Δ_u	Failure mode	β	$F_{u,\ pred.}$	$F_{u,pred}/F_{u,FE}$
1	Ferritic	75	3	25	100	220	74.1	53.1	Mode 1	0.05	103.55	1.40
2	Ferritic	70	3	30	100	220	75.8	66.2	Mode 1	0.04	75.70	1.00
3	Ferritic	60	3	40	100	220	85.2	98.5	Mode 1	0.03	72.08	0.85
4	Ferritic	50	3	50	100	220	76.6	72.5	Mode 1	0.03	94.79	1.24
5	Ferritic	40	3	60	100	220	76.5	98.5	Mode 1	0.02	69.01	0.90
6	Ferritic	30	3	70	100	220	65.6	79.0	Mode 1	0.02	68.25	1.04
7	Ferritic	25	3	75	100	220	56.0	63.0	Mode 1	0.02	44.48	0.79
8	Ferritic	75	6	25	100	220	158.4	28.9	Mode 1	0.21	150.43	0.95
9	Ferritic	70	6	30	100	220	153.7	30.5	Mode 1	0.18	112.89	0.73
10	Ferritic	60	6	40	100	220	147.1	42.9	Mode 1	0.13	98.43	0.67
11	Ferritic	50	6	50	100	220	132.9	41.2	Mode 1	0.11	115.40	0.87
12	Ferritic	40	6	60	100	220	124.2	44.3	Mode 1	0.09	86.15	0.69
13	Ferritic	30	6	70	100	220	117.7	48.0	Mode 1	0.08	83.09	0.71
14	Ferritic	25	6	75	100	220	121.2	78.0	Mode 1	0.07	106.63	0.88
15	Ferritic	75	9	25	100	220	193.9	15.3	Mode 1	0.48	228.56	1.18
16	Ferritic	70	9	30	100	220	183.9	20.1	Mode 1	0.40	174.87	0.95
17	Ferritic	60	9	40	100	220	165.2	26.4	Mode 1	0.30	142.34	0.86
18	Ferritic	50	9	50	100	220	147.2	31.5	Mode 1	0.24	149.76	1.02
19	Ferritic	40	9	60	100	220	133.9	34.6	Mode 1	0.20	114.71	0.86
20	Ferritic	30	9	70	100	220	116.6	37.4	Mode 1	0.17	107.82	0.92
21	Ferritic	25	9	75	100	220	111.2	37.9	Mode 1	0.16	113.94	1.02
22	Ferritic	75	12	25	100	220	205.2	7.7	Mode 2	0.86	256.67	1.25
23	Ferritic	70	12	30	100	220	197.0	9.5	Mode 2	0.72	224.86	1.14
24	Ferritic	60	12	40	100	220	178.0	14.4	Mode 1	0.54	203.82	1.15
25	Ferritic	50	12	50	100	220	159.6	19.9	Mode 1	0.43	197.85	1.24
26	Ferritic	40	12	60	100	220	141.3	25.1	Mode 1	0.36	154.69	1.09
27	Ferritic	30	12	70	100	220	121.6	29.1	Mode 1	0.31	142.45	1.17
28	Ferritic	25	12	75	100	220	117.5	35.7	Mode 1	0.29	162.76	1.39
29	Ferritic	75	15	25	100	220	225.9	7.8	Mode 2	1.34	256.32	1.13

30	Ferritic	70	15	30	100	220	216.8	9.5	Mode 2	1.12	245.09	1.13
31	Ferritic	60	15	40	100	220	199.5	11.3	Mode 2	0.84	231.04	1.16
32	Ferritic	50	15	50	100	220	176.0	14.4	Mode 2	0.67	214.27	1.22
33	Ferritic	40	15	60	100	220	157.4	17.7	Mode 2	0.56	191.66	1.22
34	Ferritic	30	15	70	100	220	139.1	25.1	Mode 2	0.48	169.05	1.22
35	Ferritic	25	15	75	100	220	139.2	41.6	Mode 2	0.45	157.75	1.13
											Average	1.03
											St. dev	0.20

6. Conclusions

A comprehensive numerical study on the structural behaviour of stainless steel bolted T-stubs fabricated from EN 1.4003 ferritic stainless steel grade is reported herein. The numerical study details the development of an FE model, which takes into account the recorded material anisotropy and employs a quasi-static explicit dynamic solution scheme to overcome convergence difficulties. The developed model is validated against the experimental results reported in the companion paper [35]. The validation is carried out by comparing the numerical to the experimental results in terms of plastic resistance, ultimate resistance and ultimate displacements, as well as overall load deformation response. A comparison of the results obtained from the models employing a general static analysis method with those based on an explicit dynamic analysis has been reported. The effect of changing the number of elements in the mesh through the flange thickness was revealed. Moreover, the failure modes obtained from numerical study was compared with the experimental response and comprehensively reported. The effect of incorporating the material anisotropy into the FE model was studied and it was concluded that the plastic force predictions are very accurate and more consistent when material anisotropy is considered.

Based on the validated model, stress distributions through the thickness of the flange at various locations along the length of the T-stub models were obtained at load levels corresponding to the plastic and the ultimate resistance of the T-stub. The obtained results confirmed observations made in the companion paper [35] regarding the prevailing load transfer mechanism changing form flexural to membrane at high deformations. Furthermore, the actual stress values at which the plastic resistance load is reached were found to be close to the ultimate tensile stress at the extreme fibres of the T-stubs. It is thus believed that the main source of overstrength observed for T-stubs is not the strain hardening at the developed yield lines but the membrane action (and strain hardening) occurring at high deformation values. This significant reserve strength may be important in enhancing the robustness of structures. Subsequently, the developed FE model which explicitly considers damage provides accurate predictions for the available ductility and fracture of the stainless steel bolted T-stubs in tension. It was concluded that neglecting the propagation of damage in the FE models leads to conservative predictions for the displacement of fracture and the FE model although computationally less costly cannot accurately simulate the behaviour of the T-stubs near and after their peak resistance, yields however predictions with a reasonable level of conservatism, suitable for design purposes.

Moreover, the attained plastic resistance forces from the developed FE models are in a good agreement with plastic resistance predictions based on EN 1993-1-8 [1]. This was attributed to similar strain-hardening characteristics of ferritic stainless steels and carbon steel. The plastic resistances of the ferritic T-stubs were well predicted by EN 1993-1-8 [1].

Finally, the proposed expressions for ultimate resistance predictions of bolted T-stubs made of carbon steel by Tartaglia et al. [48] which take into account the effect of membrane actions, were confirmed against the available test data for austenitic and duplex stainless steel bolted T-stubs [20, 33] and numerical parametric study results on ferritic stainless steel T-stubs. The ultimate resistance predictions were obtained with a consistent accuracy for austenitic and duplex stainless steel T-stubs which exhibited failure mode 1 and mode 2 by the proposed formula. The mean value of predicted and experimental ultimate force is 0.97 with a standard deviation of 0.11. Similarly, the proposed predictive model was shown to predict the ultimate resistance of the ferritic stainless steel T-stubs with the overall ratio of predictive ultimate forces and the parametric study results as 1.03 with a COV value of 0.20 which clearly shows that the proposed expressions provide on average good ultimate force predictions for ferritic stainless steel bolted T-stubs. The predictions were satisfactory in overall with a COV value of 0.20, yet it overpredicted the ultimate resistances of the T-stubs which exhibited failure mode 2 or very close to the failure mode 3, since originally, the developed equations were intended to be used for T-stubs failing predominantly in mode 1.

References

[1] EN 1993-1-8. Eurocode 3: Design of steel structures – Part 1-8: Design of joints. CEN. 2005.

[2] Bursi OS, Jaspart JP, Benchmarks for finite element modelling of bolted steel connections, *J. Constr. Steel Res*. 43 (1997) 17–42.

[3] Zajdel, M. _1997_. “Numerical analysis of bolted tee-stub connections.” *TNO-Rep. No. 97-CON-R-1123*.

[4] Gebbeken, N., Wanzek, T., and Petersen, C. _1997_. “Semi-rigid connections, T-stub model-Report on experimental investigations.” *Rep. No. 97/2*, Institut für Mechanik und Static, Univ. des Bundeswehr München, Munich, Germany.

[5] Mistakids ES, Baniotopoulos CC, Bisbos CD, Panagiotopoulos PD, Steel T-stub connections under static loading: an effective 2-D numerical model, *J. Constr. Steel Res*. 44 (1997) 51–67.

[6] Swanson JA, Kokan DS, Leon RT, Advanced finite element modelling of bolted T-stub connection components, J. Constr. Steel Res. 58 (2002) 1015–1031.

[7] Gantes CJ, Lemonis ME, Influence of equivalent bolt length in finite element modelling of T-stub steel connections, *Comput. Struct*. 81 (2003) 595–604.

[8] Coelho AMG, Silva LSD, Bijlaard FSK, Finite-element modelling of the nonlinear

behaviour of bolted T-stub connections, J. Struct. Eng. 132 (2006) 918–928.

[9] Coelho AMG, Silva LSD, Bijlaard FSK. Ductility analysis of bolted extended end plate beam-to-column connections in the framework of the component method. *Steel Compos Struct* 2006;6:33–53. doi:10.12989/scs.2006.6.1.033.

[10] Herrera RA, Bravo M, Gómez G, Aedo G, Performance of built-up T-stubs for double T moment connections, *J. Constr. Steel Res*. 88 (2013) 289–295.

[11] Hantouche EG, Kukreti AR, Rassati GA, Investigation of secondary prying in thick built-up T-stub connections using nonlinear finite element modelling, Eng. Struct. 36 (2012) 113–122.

[12] Hantouche EG, Kukreti AR, Rassati GA, Prying models for strength in thick-flange built-up T-stubs with complete joint penetration and fillet welds, *J. Struct. Eng*. 141 (2014) 1–6.

[13] Abidelah A, Bouchair A, Kerdal DE, Influence of the flexural rigidity of the bolt on the behaviour of the T-stub steel connection, *Eng. Struct*. 81 (2014) 181–194.

[14] Francavilla AB, Latour M, Piluso V, Rizzano G, Simplified finite element analysis of bolted T-stub connection components, *Eng. Struct*. 100 (2015) 656–664.

[15] Ceniceros JF, Garcia AS, Torres FA, Pison FJMDA, numerical-informational approach for characterising the ductile behaviour of the T-stub component. Part 1: refined finite element model and test validation, *Eng. Struct*. 82 (2015) 236–248.

[16] Ceniceros JF, Garcia AS, Torres FA, Pison FJMDA, numerical-informational approach for characterising the ductile behaviour of the T-stub component. Part 2: parsimonious soft-computing-based metamodel, Eng. Struct. 82 (2015) 249–260.

[17] Kon Z, Kim S-E. Numerical estimation for initial stiffness and ultimate moment of T-stub connections. *Journal of Constructional Steel Research* 2018;141:118–31. https://doi.org/10.1016/j.jcsr.2017.11.008.

[18] Gödrich L, Wald F, Kabeláč J, Kuříková M. Design finite element model of a bolted T-

stub connection component. *Journal of Constructional Steel Research* 2019;157:198–206. https://doi.org/10.1016/j.jcsr.2019.02.031.

[19] Bouchair A, Averseng J, Abidelah A. Analysis of the behaviour of stainless steel bolted connections. *J Constr Steel Res* 2008;64:1264–74. doi:10.1016/j.jcsr.2008.07.009.

[20] Yuan HX, Hu S, Du XX, Yang L, Cheng XY, Theofanous M. Experimental behaviour of stainless steel bolted T-stub connections under monotonic loading. *J Constr Steel Res* 2019;152:213–24.

[21] Elflah M, Theofanous M, Dirar S, Yuan HX. Behaviour of stainless steel beam-tocolumn joints—Part 1: Experimental investigation. *J Constr Steel Res* 2019;152:183–93.

[22] Elflah M, Theofanous M, Dirar S. Behaviour of stainless steel beam-to-column joints—Part 2: Numerical modelling parametric study. *J Constr Steel Res* 2019;152:194–212.

[23] Elflah M, Theofanous M, Dirar S, Yuan HX. Structural behaviour of stainless steel beam-to-tubular column joints. *Engineering Structures* 184: 158-175.

[24] EN 1993-1-4:2006+A1:2015, Eurocode 3: Design of Steel Structures–Part 1.4: General Rules–Supplementary Rules for Stainless Steels, CEN. 2015.

[25] Wang, J., Uy, B. and Li, D. (2019), "Behaviour of large fabricated stainless steel beam-to-tubular column joints with extended endplates", *Steel Compos. Struct., Int. J.*, 32(1), 141-156. https://doi.org/10.12989/scs.2019.32.1.141

[26] Bu, Y., Wang, Y. and Zhao, Y. (2019) Study of stainless steel bolted extended end-plate joints under seismic loading. *Thin-Walled Structures*, 144: 106255. doi:10.1016/j.tws.2019.106255.

[27] Song, Y. & Uy, B. and Wang, J. (2019). Numerical analysis of stainless steel-concrete composite beam-to-column joints with bolted flush endplates. *Steel and Composite Structures*. 33. 975-994. 10.12989/scs.2019.33.1.975.

[28] Gao, J. D., Yuan, H. X., Du, X. X., Hu, X. B. & Theofanous, M. Structural behaviour of

stainless steel double extended end-plate beam-to-column joints under monotonic loading. Thin-Walled Structures 151, 106743 (2020), doi: 10.1016/j.tws.2020.106743.

[29] Gao JD, Du XX, Yuan HX, Theofanous M. Hysteretic performance of stainless steel double extended end-plate beam-to-column joints subject to cyclic loading. Thin-Walled Structures 2021;164:107787. https://doi.org/10.1016/j.tws.2021.107787.

[30] Yapici O, Theofanous M, Dirar S, Yuan H. Behaviour of Ferritic Stainless Steel Bolted T-stubs Under Tension-Part 1: Experimental Investigations. Ce/Papers 2021;4:866–75. https://doi.org/10.1002/cepa.1372.

[31] Yapici O, Theofanous M, Dirar S, Yuan H. Behaviour of Ferritic Stainless Steel Bolted T-stubs Under Tension-Part 2: Numerical Investigations. Ce/Papers 2021;4:876–85. https://doi.org/10.1002/cepa.1373.

[32] Yapici O, Theofanous M, Afshan S, Yuan H, Dirar S. Numerical modelling of stainless steel bolted T-stubs in tension. Thin-Walled Structures 2022;177:109432. https://doi.org/10.1016/j.tws.2022.109432.

[33] Yuan HX, Gao JD, Theofanous M, Yang L, Schafer BW. Initial stiffness and plastic resistance of bolted stainless steel T-stubs in tension. Journal of Constructional Steel Research 2020;173:106239. https://doi.org/10.1016/j.jcsr.2020.106239.

[34] Yuan HX, Liu XH, Liu JL, Theofanous M. Cyclic behaviour and hysteretic model of austenitic stainless steel bolted T-stubs. Journal of Constructional Steel Research 2021;182:106659. https://doi.org/10.1016/j.jcsr.2021.106659

[35] Yapici O, Theofanous M, Yuan H, Skalomenos K, Dirar S. Experimental study of ferritic stainless steel bolted T-stubs under monotonic loading. Journal of Constructional Steel Research 2021;183:106761. https://doi.org/10.1016/j.jcsr.2021.106761.

[36] Hibbitt H, Karlsson B, Sorensen P, ABAQUS Analysis User's Manual Version 6.10, Dassault Systèmes Simulia Corp.: Providence, RI, USA, 2011.

[37] Wang, Z., Tizani, W. and Wang, Q. (2010) Strength and initial stiffness of a blind-bolt connection based on the T-stub model. *Engineering structures*, 32: (9): 2505-2517.

[38] Liu, Y., Malaga-Chuquitaype, C. and Elghazouli, A.Y. (2012b) Response and component characterisation of semi-rigid connections to tubular columns under axial loads. *Engineering structures*, 41: 510-532.

[39] Massimo, L., Gianvittorio, R., Aldina, S., et al. (2014) Experimental analysis and mechanical modeling of T-stubs with four bolts per row. *Journal of Constructional Steel Research*, 101: 158-174.

[40] De Matteis G, Mandara A, Mazzolani FM. T-stub aluminium joints: influence of behavioural parameters. *Comput Struct* 2000;78(1–3):311–27.

[41] Wang, Z.-Y. and Wang, Q.-Y. (2016) Yield and ultimate strengths determination of a blind bolted endplate connection to square hollow section column. *Engineering Structures,* 111: 345-369.

[42] Quach, W., Teng, J.G. and Chung, K. (2008) Three-stage full-range stress-strain model for stainless steels. *Journal of structural engineering*, 134: (9): 1518-1527.

[43] Becque, J, Oyawoye, A, Guadagnini, M, Huang, S. Notched Strip Tensile Tests to Determine Yield Characteristics of Stainless Steel. *Journal of Engineering Mechanics* 2014;140:04013007.

[44] Hill, R. (1953). “A new method for determining the yield criterion and plastic potential of ductile metals.” *J. Mech. Phys. Solids*, 1(4), 271–276.

[45] Salih, E.L., Gardner, L. and Nethercot, D.A. (2010) Numerical investigation of net section failure in stainless steel bolted connections. *Journal of Constructional Steel Research*, 66: (12): 1455-1466.

[46] Pavlović M, Marković Z, Veljković M, Buđevac D. Bolted shear connectors vs. headed studs behaviour in push-out tests. *Journal of Constructional Steel Research* 2013;88:134–49.

https://doi.org/10.1016/j.jcsr.2013.05.003.

[47] Yapici O (2021). Ultimate response of stainless steel bolted connections, The University of Birmingham, PhD dissertation. http://etheses.bham.ac.uk/id/eprint/11892

[48] Tartaglia R, D'Aniello M, Zimbru M. Experimental and numerical study on the T-Stub behaviour with preloaded bolts under large deformations. *Structures* 2020;27:2137–55. https://doi.org/10.1016/j.istruc.2020.08.039.